

**COMPARISON OF ABSOLUTE DOSE FROM THERAPEUTIC
PHOTON BEAMS IN A CHEST RANDO PHANTOM:
TREATMENT PLANNING CALCULATION,
MONTE CARLO SIMULATION,
AND TLD MEASUREMENT**

WASUMA RAKKRAI

**A THESIS SUBMITTED IN PARTIAL FULLFILLMENT
OF THE REQUIREMENTS FOR
THE DEGREE OF MASTER OF SCIENCE (MEDICAL PHYSICS)
FACULTY OF GRADUATE STUDIES
MAHIDOL UNIVERSITY
2012**

COPYRIGHT OF MAHIDOL UNIVERSITY

Thesis
entitled
**COMPARISON OF ABSOLUTE DOSE FROM THERAPEUTIC
PHOTON BEAMS IN A CHEST RANDO PHANTOM:
TREATMENT PLANNING CALCULATION,
MONTE CARLO SIMULATION,
AND TLD MEASUREMENT**

.....
Miss Wasuma Rakkrai
Candidate

.....
Assoc. Prof. Vipa Boonkitticharoen,
Ph.D. (Radiation Biology)
Major advisor

.....
Asst. Prof. Nakorn Phaisangittisakul,
Ph.D. (Physics)
Co-advisor

.....
Prof. Banchong Mahaisavariya,
M.D., Dip Thai Board of Orthopedics
Dean
Faculty of Graduate Studies
Mahidol University

.....
Lect. Puangpen Tangboonduangjit,
Ph.D. (Medical radiation Physics)
Program Director
Master of Science Program
in Medical Physics
Faculty of Medicine
Ramathibodi Hospital
Mahidol University

Thesis
entitled
**COMPARISON OF ABSOLUTE DOSE FROM THERAPEUTIC
PHOTON BEAMS IN A CHEST RANDO PHANTOM:
TREATMENT PLANNING CALCULATION,
MONTE CARLO SIMULATION,
AND TLD MEASUREMENT**

was submitted to the Faculty of Graduate Studies, Mahidol University
for the degree of Master of Science (Medical Physics)

on
May 21, 2012

.....
Miss Wasuma Rakkrai
Candidate

.....
Asst. Prof. Nakorn Phaisangittisakul,
Ph.D. (Physics)
Member

.....
Assoc. Prof. Sivalee Suriyapee,
M.Eng. (Nuclear Technology)
Chair

.....
Lect. Puangpen Tangboonduangjit,
Ph.D. (Medical radiation Physics)
Member

.....
Assoc. Prof. Vipa Boonkitticharoen,
Ph.D. (Radiation Biology)
Member

.....
Prof. Banchong Mahaisavariya,
M.D., Dip Thai Board of Orthopedics
Dean
Faculty of Graduate Studies
Mahidol University

.....
Prof. Winit Puapradit,
M.D., M.P.H.
Dean
Faculty of Medicine
Ramathibodi Hospital
Mahidol University

ACKNOWLEDGEMENTS

This thesis would not have been possible without the support, patience and guidance of the following people. First, I would like to express my sincere gratitude and deep appreciation to my thesis advisors, Assoc. Prof. Dr.Vipa Boonkitticharoen and Asst. Prof. Dr.Nakorn Phaisangittisakul, for their guidance, suggestions and encouragement. I am equally grateful to Asst. Prof. Chirapha Tannanonta for her kindness, good advice, and suggestion in the measurement.

I am deeply grateful to Assoc. Prof.Sivalee Suriyapee and Dr. Puangpen Tangboonduangjit for their kindness in examining the thesis defense and providing suggestions for its improvement.

The major experiment material for this study, Linac, Rando phantom, TLDs and a personal computer were provided by Division of Radiation Oncology Ramathibodi Hospital, Division of Radiation Oncology Chulabhorn Hospital and Department of Physics, Faculty of Science, Chulalongkorn University. I appreciate their support.

I am also indebted to all the teachers, lecturers and staffs at the School of Medical Physics, Ramathibodi Hospital, mahidol University for their kind support and teaching me in the Medical Physics program. I also wish to thank my classmates in the School of Medical Physics for their help and encouragement thought the entire course of study

I am also thankful to my friends, Miss Patchareporn Dechsupa and Mr. Wuttichai Boonrat, for training me in Monte Carlo simulation and for their continual support and friendship.

Finally, and most importantly, I would like to thank my family for their unconditional support and encouragement throughout my life. Without you none of this would have been possible.

Wasuma Rakkrai

COMPARISON OF ABSOLUTE DOSE FROM THERAPEUTIC PHOTON
BEAMS IN A CHEST RANDO PHANTOM: TREATMENT PLANNING
CALCULATION, MONTE CARLO SIMULATION, AND TLD
MEASUREMENT

WASUMA RAKKRAI 5036368 RAMP/M

M.Sc. (MEDICAL PHYSICS)

THESIS ADVISORY COMMITTEE: VIPA BOONKITTICHAROEN, Ph.D.
(RADIOBIOLOGY), NAKORN PHAISANGKITTISAKUL, Ph.D. (PHYSICS)

ABSTRACT

The aim of this study was to assess the absorbed dose in a chest Rando phantom by performing the measurement using TLDs, calculation with Collapse Cone Convolution (CCC) algorithm and simulation with Monte Carlo (MC). For evaluating the dose calculation algorithm, the CT data of a Rando phantom were transferred to the Monte Carlo software (EGSnrc code) by using the CTCREATE code to convert the phantom's CT data to the material types and mass densities. The absorbed doses were simulated for two opposing fields of 6 and 10 MV photon beams, AP-PA and RAO-LPO. Since the output dose from MC simulation is dose in the voxel per incident particle, we have developed the formalism to obtain an absolute dose from the simulated dose. To investigate the reliability of MC absolute dose calculation, the simulations were performed for some square and rectangular fields in water phantom and then the results were compared with the measurement. The comparison shows good agreement between the calculated and the measured doses with the percentage difference of less than 2%. The dose from the identical beam-setup was calculated by the treatment planning system. The point doses in various locations in the chest Rando phantom were measured using the LiF TLDs. For dose comparison in the Rando phantom, we found that the dose obtained by MC agrees better with the measurement than that of the treatment planning within the beam region for both inhomogeneous and interface locations. However, large deviation in the region of the outer beam, where the dose gradient is high or beam edge where the dose is quite small, was observed. The disagreements might be improved by better matching of the parameters of the beam model from the machine.

KEY WORDS: MONTE CARLO SIMULATION/ TREATMENT PLANNING/
PHOTON DOSE CALCULATION/ CHEST RANDO PHANTOM

63 pages

การเปรียบเทียบปริมาณรังสีจากลำรังสีโฟตอนในบริเวณทรวงอกของ RANDO PHANTOM จากโปรแกรมการวางแผนการรักษา การจำลองมอนติคาร์โล และการวัดด้วยทีแอลดี

COMPARISON OF ABSOLUTE DOSE FROM THERAPEUTIC PHOTON BEAMS IN A CHEST RANDO PHANTOM: TREATMENT PLANNING CALCULATION, MONTE CARLO SIMULATION, AND TLD MEASUREMENT

วสุมารักไคร่ 5036368 RAMP/M

วท.ม. (ฟิสิกส์การแพทย์)

คณะกรรมการที่ปรึกษาวิทยานิพนธ์: วิชา บุญกิตติเจริญ, Ph.D. (RADIOBIOLOGY), นคร ไพศาลกิตติสกุล, Ph. D (PHYSICS)

บทคัดย่อ

วัตถุประสงค์ของงานวิจัยนี้คือเพื่อตรวจสอบปริมาณรังสีดูดกลืนในบริเวณทรวงอกของ Rando phantom ด้วยการวัดโดยใช้ Thermoluminescence dosimeter (TLD) ด้วยการจำลองแบบมอนติคาร์โล และการคำนวณด้วยโปรแกรมการวางแผนการรักษาที่ใช้ Collapse Cone Convolution algorithm ในการตรวจสอบปริมาณรังสีที่ได้จากการจำลอง เริ่มด้วยการแปลงข้อมูลภาพที่ได้จากการสแกน Rando phantom จากเครื่องเอกซเรย์คอมพิวเตอร์ โดยใช้โปรแกรม CTCREATE ในการเปลี่ยนข้อมูลเลข CT ของแต่ละ voxel ไปเป็นค่าความหนาแน่นเพื่อใช้ในการจำลองหาปริมาณรังสีด้วยโปรแกรม DOSXYZnrc และใช้ข้อมูลภาพชุดเดียวกันนี้ในโปรแกรมการวางแผนการรักษาและคำนวณปริมาณรังสี ในการศึกษาสนใจลักษณะการฉายลำรังสีแบบ two opposing fields ในแบบ AP-PA และ RAO-LPO เนื่องจากค่าปริมาณรังสีที่ได้จากการจำลองด้วยเทคนิคมอนติคาร์โลเป็นค่าปริมาณรังสีต่อจำนวนอนุภาคที่ตกกระทบกับเป้า จึงได้พัฒนาวิธีการเพื่อแปลงปริมาณดังกล่าวให้เป็นปริมาณรังสีดูดกลืน แล้วจึงทำการตรวจสอบความถูกต้องโดยการเปรียบเทียบค่าที่ได้จากการจำลองหาปริมาณรังสีดูดกลืนในน้ำเทียบกับการวัดที่ขนาดของลำรังสีแบบจตุรัสและแบบผืนผ้าหลายขนาด พบว่ามีค่าความแตกต่างของการคำนวณกับการวัดน้อยกว่า 2% แสดงว่าวิธีการแปลงค่าปริมาณรังสีดังกล่าวมีความน่าเชื่อถือ ในการเปรียบเทียบกับปริมาณรังสีดูดกลืนใน Rando phantom ที่ได้จากการจำลองแบบมอนติคาร์โล ที่วัดด้วย LiF TLDs และที่คำนวณจากโปรแกรมการวางแผนการรักษา โดยทั่วไปแล้วพบว่าปริมาณรังสีที่ได้จากการคำนวณด้วยเทคนิคมอนติคาร์โลมีค่าใกล้เคียงกับการวัดมากกว่าค่าที่ได้จากการคำนวณด้วยโปรแกรมการวางแผนการรักษาในบริเวณพื้นที่ในขอบเขตของลำรังสี ถึงแม้ว่าจะมีบริเวณที่เป็นรอยต่อระหว่างเนื้อเยื่อสองชนิดที่มีค่าความหนาแน่นต่างกันค่อนข้างมาก นอกจากนี้พบว่าที่บริเวณขอบของลำรังสีและนอกพื้นที่ลำรังสีซึ่งเป็นบริเวณที่มีการเปลี่ยนแปลงของปริมาณรังสีสูงและมีปริมาณรังสีต่ำ ปริมาณรังสีจากการคำนวณด้วยเทคนิคมอนติคาร์โลจะให้ค่าที่ต่างจากการวัดสูงเกินค่าที่ยอมรับได้ ซึ่งค่าความแตกต่างดังกล่าวอาจจะแก้ไขได้โดยการปรับค่าพารามิเตอร์ที่ใช้ในขั้นตอนการสร้างแบบจำลองของเครื่องเร่งอนุภาคให้สอดคล้องกับข้อมูลการวัดมากขึ้น

CONTENTS

	Page
ACKNOWLEDGEMENTS	iii
ABSTRACT (ENGLISH)	iv
ABSTRACT (THAI)	v
LIST OF TABLES	vii
LIST OF FIGURES	ix
LIST OF ABBREVIATIONS	xi
CHAPTER I INTRODUCTION	1
CHAPTER II OBJECTIVES	9
CHAPTER III LITERATURE REVIEWS	10
CHAPTER IV MATERIALS AND METHODS	14
CHAPTER V RESULTS AND DISCUSSIONS	31
CHAPTER VI CONCLUSIONS	50
REFERENCES	52
APPENDICES	55
Appendix A	56
Appendix B	58
BIOGRAPHY	63

LIST OF TABLES

Tables	Page
1.1 Estimates of Uncertainty (in terms of one standard deviation) in absolute dose in the patient for the complete treatment procedure using megavoltage photons.	5
1.2 The suggestion of acceptability criteria for external beam dose calculations.	7
4.1 Field sizes and depth used in the verification of the dose-MU equation.	25
5.1 Relative dose obtained from MC simulations (normalized by the number of electrons incident on the target).	31
5.2(a) The doses from MC calculation and measurement at a depth of maximum dose (d_{\max})	32
5.2(b) The doses from MC calculation and measurement at 5 cm depth	33
5.2(c) The doses from MC calculation and measurement at 10 cm depth	33
5.2(d) The doses from MC calculation and measurement at 20 cm depth	34
5.3 Individual element correction coefficient (ECC_i) value for each TLD	36
5.4 The corrected individual element correction coefficient (ECC_{ci}) value for each TLD	37
5.5 Absorbed doses in the RANDO phantom measured by the TLDs for AP-PA fields.	39
5.6 Monte Carlo and Pinnacle dose calculation compared with measured TLD dose: 6 MV photon beam, AP-PA technique.	40
5.7 Monte Carlo and Pinnacle dose calculation compared with measured TLD dose: 10 MV photon beam, AP-PA technique.	41
5.8 Absorbed doses in the RANDO phantom measured by the TLDs for RAO-LPO fields.	44

LIST OF TABLES (cont.)

Tables	Page
5.9 Monte Carlo and Pinnacle dose calculation compared with measured TLD dose: 6 MV photon beam, RAO-LPO technique.	45
5.10 Monte Carlo and Pinnacle dose calculation compared with measured TLD dose: 10 MV photon beam, RAO-LPO technique.	46
B-1 TLDs measurement data for AP-PA fields: 6 MV	59
B-2 TLDs measurement data for AP-PA fields: 10 MV	60
B-3 TLDs measurement data for RAO-LPO fields: 6 MV	61
B-4 TLDs measurement data for RAO-LPO fields: 10 MV	62

LIST OF FIGURES

Figures	Page
1.1 The principle of therapeutic ratio. Curve A represents the tumor control probability (TCP), curve B the normal tissue complication probability (NTCP).	1
1.2 Regions for photon dose calculation agreement analysis	6
3.1 diagram of the studied phantom	11
4.1 The medical linear accelerator Varian Clinac 2100C	14
4.2a a Farmer type chamber FC65-G	15
4.2b a parallel plate chamber type 34001	15
4.2c DOSE-1 electrometer	15
4.3 The 1D water phantom from Scanditronix wellhofer	16
4.4 Computed tomography machine (Philips model MX IDT 8000)	17
4.5 The Alderson Radiation Therapy phantom (ART)	17
4.6 The CT number to density curve of 140 kVp of Phillips MX IDT 8000	19
4.7a Beam directions in two plans: AP-PA setup at beam central axis slice.	20
4.7b Beam directions in two plans: RAO-LPO setup at beam central axis slice.	21
4.8 A schematic of the linac treatment head. Part A is the fixed components of linac and part B is the variable components.	22
4.9a Field directions for AP-PA setup and showing the measurement points for the slice numbers 16.	27
4.9b Field directions for AP-PA setup and showing the measurement points for the slice numbers 17.	28

LIST OF FIGURES (cont.)

Figures		Page
4.9c	Field directions for AP-PA setup and showing the measurement points for the slice numbers 18.	28
4.10a	Field directions for RAO-LPO setup and showing the measurement points for the slice numbers 16.	29
4.10b	Field directions for RAO-LPO setup and showing the measurement points for the slice numbers 17.	29
4.10c	Field directions for RAO-LPO setup and showing the measurement points for the slice numbers 18.	30
5.1	The linearity of the TLDs	35
5.2a	Field directions for AP-PA setup and the numbers indicate the points of dose investigation for slice number 16.	42
5.2b	Field directions for AP-PA setup and the numbers indicate the points of dose investigation for slice number 17.	42
5.2c	Field directions for AP-PA setup and the numbers indicate the points of dose investigation for slice number 18.	43
5.3a	Field directions for RAO-LPO setup and the numbers indicate the points of dose investigation for slice number 16.	47
5.3b	Field directions for RAO-LPO setup and the numbers indicate the points of dose investigation for slice number 17.	47
5.3c	Field directions for RAO-LPO setup and the numbers indicate the points of dose investigation for slice number 18.	48

LIST OF ABBREVIATIONS

Abbreviation	Term
3D	Three dimension
AP	Anteroposterior
CCC	Collapse Cone Convolution
cGy	Centrigray
cm	Centimeter
cm ²	Square centrimeters
cm ³	Cubic centimeters
CT	Computed Tomography
GeV	Gigaelectron volt
GHz	Gigahertz
g/cm ³	Gram per square centrimeters
ICRU	The International Commission on Radiation Units and Measurements
IMRT	Intensity Modulated Radiation Therapy
keV	Kiloelectron volt
LPO	Left Posterior Oblique
MC	Monte Carlo
MCNP	Monte Carlo N-particle
MeV	Megaelectron volt
MU	Monitor unit
MV	Megavolt
NTCP	Normal tissue complication probability
PA	Posteroanterior
PDD	Percentage depth dose
PMMA	Polymethyl-methacrilate

LIST OF ABBREVIATIONS (cont.)

Abbreviation	Term
RAM	random access memory
RAO	Right Anterior Oblique
RTP	Radiotherapy treatment planning
SAD	Source to axis distance
SD	Standard Deviation
TAR	Tissue air ratio
TCP	Tumor control probability
TG	Task group
TLD	Thermoluminescence dosimeter
TMR	Tissue maximum ratio
TPS	Treatment planning system
TSD	Target to surface distance
V	Volt

CHAPTER I

INTRODUCTION

The aim of radiotherapy is to deliver enough radiation to destroy the tumor without introducing severe complications in the surrounding normal tissue. This aim can be described by dose-response curves for the tumor and normal tissue as shown in Figure 1.1. Effectiveness of radiotherapy depends on maximum tumor control probability (TCP) and minimum normal tissue complication probability (NTCP). Both of these quantities are very sensitive to absorbed dose. Providing 5% change in dose, 10-20% will change in TCP and NTCP will change up to 20-30% [1]. Thus the accuracy in dose calculation must be concerned.

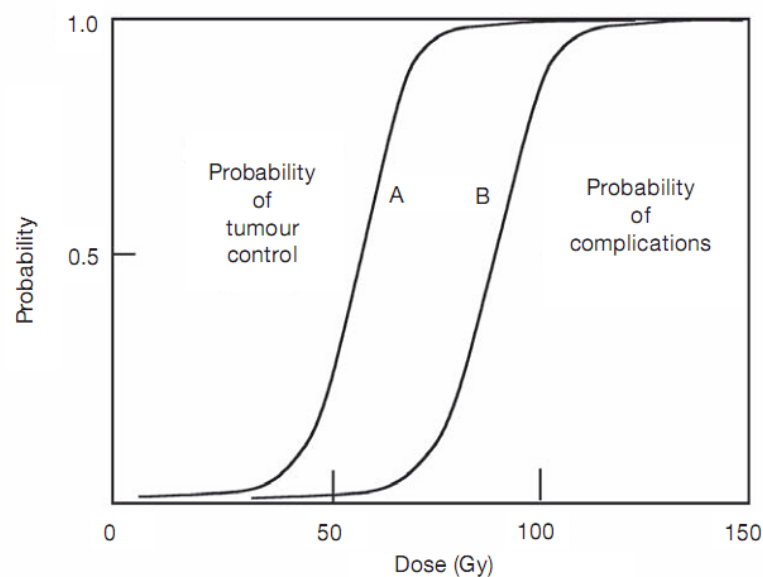


Figure 1.1 The principle of therapeutic ratio. Curve A represents the tumor control probability (TCP), curve B the normal tissue complication probability (NTCP) [2].

1.1 Computerized treatment planning systems

Computerized treatment planning system (TPS) has been used in external beam radiotherapy to generate optimal beam shapes and directions incident on the patient. By this technique, it leads to maximizing tumor control and minimizing normal tissue morbidity. The process of treatment planning system involves many steps and dose calculation algorithm is the most important part in a TPS. This part is very complicate and requires high accuracy so TPS has to be verified before starting to use with patient.

In this study, the ADAC's Pinnacle [3] which uses a Collapse Cone Convolution (CCC) Superposition computation was applied to determine the dose in patients from external photon beams. The Pinnacle planning system has three types of algorithm, Fast Convolution, Adaptive Convolution and Collapse Cone Convolution.

Fast Convolution performs a convolution superposition calculation with fewer ray directions used for the scatter calculation than those are used for Adaptive Convolution. The Fast Convolve computation is less accurate near the surface and also in the penumbra region in which the maximum error is typically less than 5%.

Adaptive Convolution performs adaptive sampling during convolution dose calculation. This algorithm reduces a computation time by sampling every fourth point in the dose grid and interpolating dose in flat areas. If the dose grid cannot be interpolated accurately enough by such sampling, Pinnacle3 automatically switches to Collapse Cone Convolution and samples every point in the dose grid.

Collapse Cone Convolution Superposition (CCCS) performs a full convolution superposition calculation that manipulates the effects of patient heterogeneities on both primary and secondary scattered radiations. The CCCS algorithm can account for the effects of beam modifiers, the external patient contour, and tissue heterogeneities on the dose distribution. The CCCS dose model consists of four parts.

i. Modeling the incident energy fluence

The incident energy fluence distribution is modeled as a two-dimensional array which describes the radiation exiting the head of the linear accelerator. This array can be adjusted to account for the flattening filters, the accelerator head, and

beam modifiers such as blocks and wedges, which shape the beam. The off-focus scatter produced in the accelerator head is modeled by defining a 2D Gaussian function as a scatter source and adjusting the incident energy fluence based on the portion of the Gaussian distribution visible from each point in the incident energy fluence plane. The geometric penumbra is modeled by convolving the array with a focal spot blurring function. The beam modifiers such as wedges and compensators are included in the array by attenuating the energy fluence by the corresponding thickness of the modifier. For static wedges and compensators, a radiological depth array is also stored which allows for proper modeling of the beam hardening due to the presence of the beam modifiers during the projection of the incident fluence array.

ii. Projection of this energy fluence through patient density

The incident energy fluence plane is projected through the CT patient representation and attenuated using mass attenuation coefficients. These coefficients are stored in a three-dimensional lookup table as a function of density, radiological depth, and off-axis angle. Patient heterogeneities are taken into account with the density dependence. Beam hardening through the patient is accounted for the radiological depth dependence, and the off-axis softening of the energy spectrum is produced with the off-axis angle dependence. To account for the changes in the photon energy spectrum at different locations in the beam, the mass attenuation coefficient lookup table is produced using a weighted sum of several mono-energetic tables.

The TERMA (Total Energy Released per unit Mass) volume is computed by projecting the incident energy fluence through the patient density volume using a ray-tracing technique. The direction of ray is determined based on the position of the radiation source and the particular location in the incident fluence plane. At each voxel in the ray path, the TERMA is computed using the attenuated energy fluence along the ray and the mass attenuation coefficient at the particular density, radiological depth, and off-axis angle.

iii. 3D superposition of an energy deposition kernel

The three-dimensional dose distribution in the patient is computed by superposition of the TERMA volume with the energy deposition kernel. The kernel represents the spread of energy from the primary photon interaction site throughout the associated volume. Poly-energetic kernels are produced by combining a series of Monte Carlo-generated mono-energetic energy deposition kernels. The superposition is carried out using a ray tracing technique similar to that used in the projection of the incident energy fluence. The kernel is inverted so that the dose can be computed in only a portion of the patient (TERMA) volume if desired.

The rays from the dose deposition site are cast in three dimensions. At each voxel of the TERMA traversed along a ray, the contribution of dose to the dose deposition site is computed and accumulated using the TERMA and the kernel value at the current radiological distance. The dose computation described above determines the dose from a single beam. Multiple beams are computed independently and the entire 3D dose distribution is created by adding the dose from each beam together according to the corresponding beam weight.

iv. Electron contamination model

Although the primary source of dose to the patient is through photons, contamination from electrons is significant to the dose near the surface of the TERMA volume. The electron dose contribution is accounted for in the algorithm by modeling a photon only dose and comparing it to the measured dose at shallow depths. This effect is then modelled with an exponential fall-off through the depth of the irradiated mass.

1.2 Dose calculation verification

It is suggested that an overall dosimetric uncertainty of 5% is clinically acceptable for radiotherapy treatment using external beams from medical accelerators (ICRU 24). In order to meet this requirement, the uncertainty in each step in the treatment process is minimized. Table 1.1 lists the estimation of uncertainties associated with the dose delivered to the patient [1]. Since 2-3% errors in the dose

computation are factored into the total uncertainty, the overall error is about 5% or larger. As a result, the dose calculation algorithm is an essential element of the treatment process and therefore requires extensive testing before being used clinically.

Table 1.1 Estimates of Uncertainty (in terms of one standard deviation) in absolute dose in the patient for the complete treatment procedure using megavoltage photons [1].

Sources of uncertainties	Uncertainty at Present (%)	Uncertainty in Future (%)
Dose at the calibration point in water	2.5	1.0
Additional uncertainty for other points	0.6	0.3
Beam Monitor stability	1.0	0.5
Beam flatness	1.5	0.5
Patient data	1.5	1.0
Patient set up and organ motion	2.5	2.0
Overall (excluding dose calculation)	4.3	2.5
Dose calculation algorithm (multiple levels)	1.0 / 2.0 / 3.0 / 5.0	1.0 / 2.0 / 3.0
TOTAL	4.4 / 4.7 / 5.2 / 6.6	2.7 / 3.2 / 3.9

There are a number of different methods in designing and organizing the experiments and calculation verification checks to be used during commissioning of a particular calculation algorithm or individual beam verification. The TG 53[4] presents a method to characterize the accuracy of a dose calculation method similar to that used by Van Dyk et al [5]. To analyze the agreement between calculations and measurements, the dose distribution due to a delivered beam is separated into several regions, illustrated in Figure 1.2.

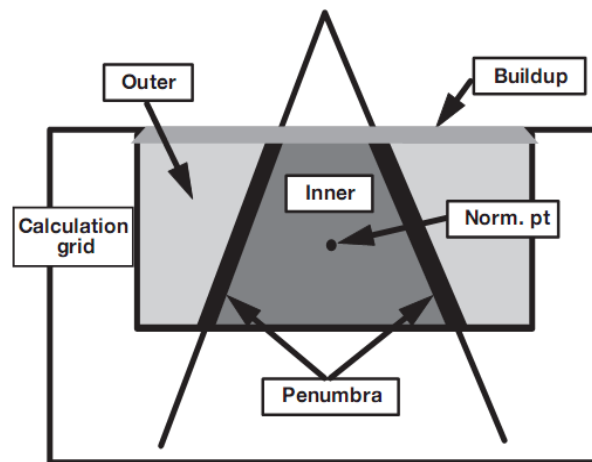


Figure 1.2 Regions for photon dose calculation agreement analysis [4]

- The inner beam (central high-dose portion of the beam)
- The penumbral region (0.5 cm inside and outside each beam/block edge)
- The outside region (outside the penumbra)
- The buildup region (from the surface to d_{\max} , both inside and outside the beam)
- The central axis
- Absolute dose at the beam normalization point

These regions should be analyzed separately. Table 1.2 illustrates the suggested analysis and examples of acceptability criteria [4]. For each situation, the accuracy of any particular algorithm or dataset may affect these expectations. The radiation oncology physicist must evaluate the expectations for each situation and determine the criteria to which the particular beam and algorithm will be compared.

Table 1.2 The suggestion of acceptability criteria for external beam dose calculations [4].

Situation	Abs.Dose @normpt (%)	Central Axis (%)	Inner Beam (%)	Penumbra (mm)	Outer Beam (%)	Buildup Region (%)
Homogeneous phantom:						
Square fields	0.5	1	1.5	2	2	20
Rectangular fields	0.5	1.5	2	2	2	20
Asymmetric fields	1	2	3	2	3	20
Blocked fields	1	2	3	2	5	50
MLC-shaped fields	1	2	3	3	5	20
Wedged fields	2	2	5	3	5	50
External surface verifications	0.5	1	3	2	5	20
SSD variations	1	1	1.5	2	2	40
Inhomogeneous phantom:						
Slab inhomogeneities	3	3	5	5	5	-
3-D inhomogeneities	5	5	7	7	7	-

1.3 Monte Carlo simulation

Another method that can be used to calculate dose is Monte Carlo (MC) simulation. The Monte Carlo method is a numerical technique based on random number sampling to simulate a stochastic process, in this case, simulate the transportation of photon and electron particles through a medium. This technique considers all aspects of photon and electron transport within a heterogeneous phantom, that why it has been shown to be more accurate than any method for radiation treatment dose calculation in any target [6]. There are numerous versions of Monte Carlo code that are most frequently used for simulating radiotherapy beam such as EGSnrc, MCNP, and PENELOPE. In this work, the Monte Carlo code used for the simulations is EGSnrc code system which was developed as a part of the OMEGA project to develop the 3-D treatment planning for radiotherapy [7]. The EGSnrc package consists of many codes for simulation, the main codes of simulation are BEAMnrc and DOSXYZnrc.

BEAMnrc code system was designed to simulate the radiation beams from any radiotherapy source, such as photon and electron beams from clinical accelerators. The BEAM code produces a phase-space output of the beam (energy, charge, position, direction, and a tag called LATCH to record the particle history) at any specified plane in simulation geometry. The simulated phase space file can be used as source input for further BEAM simulations or dose calculations using the code DOSXYZ

DOSXYZnrc code system [8] was designed for adsorbed dose calculations in 3D phantom. Phantoms were created by specifying voxel size (x,y,z), materials, and outer boundaries of the phantom in a DOSXYZnrc input file. For use with CT data, a separate program CTCREATE was used to convert the patient's CT data to the desired dimensions, material types, and mass densities by using a CT number to density correlation.

According to a study in Dosimetric verification of a treatment planning system using Collapse Cone Convolution (CCC) algorithm for photon beam therapy of Ramathibodi Hospital [9], the difference between calculated and measured dose in the regions of tissue inhomogeneities, such as lung-tissue or bone-tissue interface and phantom surface, were high ($> 5\%$). Therefore, the main purpose of this study is to use the Monte Carlo technique to calculate dose in those regions and compare with those obtained from the TPS.

CHAPTER II

OBJECTIVES

The objectives of this study were:

1. To establish an equation used for absolute dose calculation by Monte Carlo method for the 6 and 10 MV photon beams delivered from a medical linear accelerator (Varian Clinac 2100C) installed at Ramathibodi Hospital.
2. To compute the absolute dose from these 6 and 10 MV photon beams in a chest Rando phantom using the Pinnacle Treatment Planning System (CCC algorithm) and MC calculation.
3. To compare the computed doses (CCC and MC) in various locations within the Rando phantom to the measured doses obtained by TLDs.

CHAPTER III

LITERATURE REVIEWS

Accurate dose calculations are essential to radiotherapy treatment planning (RTP). Following consideration of clinical data ICRU Report 24 recommended that $\pm 5\%$ accuracy was required in the delivery of absorbed dose to the target volume. It is therefore, important that the uncertainty in each step in the treatment process is minimized. The largest source of error in calculations arises from tissue inhomogeneities (such as lung or bony anatomy) and the subsequent loss of electronic equilibrium. If the tissue inhomogeneous effect is not accurately predicted during dose calculations, unacceptable errors may arise and cause underdosage of tumors or overdosage of healthy surrounding tissues. So the dose calculation algorithm is required extensive testing before being used clinically.

Carrasco et al [10] compared the measurement of PDDs and beam profiles from several detectors with the predicted dose by different algorithms (four correction-based algorithms and one based on convolution-superposition) in a heterogeneous layer phantom with lung equivalent (Figure 3.1). Additionally Monte Carlo simulations, PENELOPE code, were performed. The correction-based algorithms were the Batho, the Modified Batho, the Equivalent TAR, and the TMS Pencil Beam. The modelled based algorithm was the Collapsed Cone. The measurement of PDD curves were obtained by ionization chambers (0.6 cm^3 NE 2571 and 0.125 cm^3 PTW31002) and TLD measurement. Beam profiles were measured at three different depths: 5 cm (the interface between the Plastic water and the lung equivalent material), 10 cm (in the middle of the lung equivalent material) and 25 cm (inside the Plastic water and beyond the lung heterogeneity) with film dosimetry.

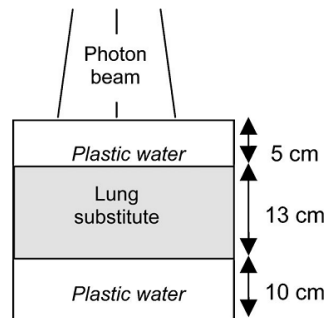


Figure 3.1 diagram of the studied phantom

For PDD curves, the results showed that only the collapse cone and the Monte Carlo simulation were correlated successfully with the measured value with a 2% averaged inside all media. However the collapse cone algorithm gave a maximum deviation value of 8% at the point closed to the first interface between the plastic water and the lung. All the correction-based calculation algorithms overestimated the dose inside the lung equivalent material. Large discrepancies were found after the second interface. For the beam profiles, all the correction-based calculation algorithms failed in the prediction inside the lung equivalent. While the collapse cone algorithm yielded more accurate result within the estimated uncertainty but it slightly overestimated the experimental value inside low density media in some cases.

Joseph R. Butts et al [11] evaluated dose calculations using the CMS Focus Clarkson, the CMS Focus Multigrid Superposition Model, the CMS Focus Fast-Fourier Transform (FFT) Convolution Model, and the ADAC Pinnacle3 Collapsed Cone Convolution Superposition Algorithms by comparing with the diode measured data. The experiment was considered in four clinical sites: pelvis, head and neck, lung and chest wall. The acceptable criterion was $\pm 4\%$ outlined by Van Dyk et al [5]. The doses delivered to the pelvis and the head and neck regions showed little difference between the algorithms' calculations. The accuracy of each algorithm fell within the acceptable criterion because both situations presented little heterogeneity and almost no missing tissue. All calculations for lung fields fell within the $\pm 4\%$ criteria of acceptability excepted in the LPO field. Delivered doses for the LPO field ranged from 4.6% low for FFT with 6 MV to 5.8% high for ADAC's algorithms with 10 MV. The Calculation of LPO field had more variation of dose because the beam passes through

low density (lung) rather than tissue with almost no buildup. For the chest wall field, there is no clinically significant difference between the calculated doses by the algorithms with the exception of the Clarkson that the differences were 6.8% and 9.1% too low for 4 and 6 MV, respectively. They concluded that the accuracy of the six algorithms ability to predict the doses for the variety of clinical situations were acceptable with the exception of using Clarkson for the chest wall. Certain algorithms were slightly better under certain conditions, but no algorithm clearly stood out for all situations.

Wyatt M. et al [12] compared the calculated dose using ADAC pinnacle³ software with the TLD measured data in a 3-D anthropomorphic phantom and with the Monte Carlo N-particle (MCNP) calculation in an idealized phantom (homogeneous distribution of 1.0 g cm^{-3} adipose tissue). The majority of differences between ADAC pinnacle³ dose calculations and TLD measurement are in the order of 5% excepted in the locations near large heterogeneities that the difference more than 5% with the maximum of 35% are obtained. The MCNP doses along the central axis of the beam were compared to Pinnacle³ point doses in the term of normalized dose. The result showed good agreement. This study showed that the dose calculation by the superposition-convolution algorithm in the area that presented large heterogeneities was not accurate when compare with the TLD measurement.

Popescu I A. et al [13] developed the formalism for absolute dose calculation for Monte Carlo simulation of radiotherapy beams. They correlated the dose accumulated in the monitor chamber with the dose in the water phantom under the standard conditions (1 cGy/MU at the depth of maximum dose, field size $10 \times 10 \text{ cm}^2$, at the machine isocenter) using the relationship between the dose scored in the monitor chamber of radiotherapy linear accelerator (linac), the number of initial particles incident on the target, and the field size and then associate 1MU with that monitor chamber dose. They found that for 6 MV photon beam, 1 MU corresponds to $8.129 \times 10^{13} \pm 1.0\%$ electron incident on the target and a total dose of $20.87 \text{ cGy} \pm 1.0\%$ in the monitor chamber of the virtual linac. They verified the accuracy of the MC absolute dose calculations by performing the measurements in a water phantom for open fields and blocked fields using an ionization chamber. A clinical 7-field dynamic IMRT head-and-neck plan which simulated on the CT data sets of a cylindrical

phantom and of a Rando phantom were measured with the ionization chamber and TLDs, respectively. The results of the simulation were in good agreement with the experiment with the percentage differences of less than 2 %. These results showed the accuracy of absolute dose calculations.

A large number of papers about the comparison of dose calculation between treatment planning system and Monte Carlo simulation have been published. Almost of them showed the comparison in term of relative doses not the actual dose to patient. So in this research, we undertake a study of dose comparison in term of absolute dose.

CHAPTER IV

MATERIALS AND METHODS

4.1 Materials

The materials used for the dose measurement consist of a linear accelerator, a Farmer type chamber FC65-G (0.65 cm^3), a parallel plate chamber type 34001, DOSE-1 electrometer and a water phantom. Thermoluminescence dosimeters (TLDs) were used to measure the dose in a Rando phantom. For dose calculations, we used Pinnacle treatment planning system and Monte Carlo software (EGSnrc code) with PC computer.

4.1.1 The linear accelerator

The linear accelerator used in the study is the Varian Clinac 2100C (Varian, Inc., Palo Alto, CA, USA) as shown in figure 4.1. The machine produces two photon beam energies with 6 and 10 MV and five electron beam energies of 6, 9, 12, 16 and 20 MeV. The stationary therapy dose rate ranges from 80 to 400 monitor units per minute which are available in five steps. Photon field sizes range from 0.5×0.5 to $40 \times 40 \text{ cm}^2$ at 100 cm target to surface distance (TSD).



Figure 4.1 The medical linear accelerator, Varian Clinac 2100C

4.1.2 Ionization chambers and Electrometer

The ionization chambers used to measure the absorbed dose and the output factor are a Farmer type chamber FC65-G and a plane parallel chamber type 34001 from PTW, respectively (Figure 4.2). The active volume of the Farmer type chamber FC65-G is 0.65cm^3 and approximately 0.35 cm^3 for the plane parallel chamber. The chambers are waterproof for use in a water phantom. Both of them were used with DOSE-1 electrometer as shown in figure 4.2. It provides two measuring modes, dose and dose rate. The adjustable high voltage ranges from -600 to 600 V.



(a)



(b)



(c)

Figure 4.2 (a) a Farmer type chamber FC65-G (b) a parallel plate chamber type 34001 (c) DOSE-1 electrometer

4.1.3 Water phantom

The water phantom from Scanditronix Wellhofer used in the experiment has the dimension of $34 \times 40 \times 35 \text{ cm}^3$ as shown in figure 4.3. It is made of acrylic plastic (PMMA) with the wall thickness of 10 mm. The position resolution within the tank is 0.1 mm.



Figure 4.3 The 1D water phantom from Scanditronix Wellhofer [15]

4.1.4 Computerized treatment planning system

The Computerized treatment planning system used in this experiment is the Pinnacle^{3®} RTPS version 7.6C [3] which is composed of a Sun UNIX workstation running the Solaris operating system and software, and a UNIX terminal emulation package on a personal computer. It provides a comprehensive set of tools for setting up and evaluating treatment plan. The patient data can be transferred from the CT workstation into the planning system. The Pinnacle RTPS is based on the convolution superposition algorithm to compute the dose distributions for photon beam including the effects of beam modifiers, the surface of the patient, and tissue heterogeneities on the dose distribution.

4.1.5 Computed tomography machine

A Philips machine model MX IDT 8000 with 64 slices illustrated in figure 4.4 was used to acquire the Rando phantom data and the information was transferred via DICOM3 to the Pinnacle planning system. The image quality depends on the level and energy of X-ray delivered to the tissue. The laser for the CT room, a set of

Gammex movable lasers, was installed at three positions, one on the ceiling and two on the opposite walls. These lasers were used for patient positioning and isocenter defining [16].



Figure 4.4 Computed tomography machine (Philips model MX IDT 8000) [17]

4.1.6 The Alderson Radiation Therapy phantom (ART)

The ART phantom as shown in figure 4.5 is modeled of tissue-equivalent material followed ICRU-44 standards. The phantom is transected-horizontally into 2.5 cm thick slices. Each slice has holes that are plugged with bone-equivalent, soft tissue-equivalent or lung tissue equivalent pins which can be replaced by TLD holder pins. The holes are drilled in grids 1.5cm×1.5cm with 5 mm diameter. The lungs are modeled from syntactic foam, with a specific density of 0.30 g/cc.



Figure 4.5 The Alderson Radiation Therapy phantom (ART) [18]

4.1.7 Thermoluminescence Dosimeter (TLD) system

4.1.7.1 The Thermoluminescence dosimeter (TLD-700)

The Thermoluminescence dosimeter (TLD-700 rods) used in the measurement is lithium fluoride (LiF) crystals doped with magnesium and titanium (LiF:Mg,Ti). The TLD-700 is composed of ^6Li and ^7Li with 0.01% and 99.99% respectively. The physical properties are rod form, with 1 mm diameter and 6 mm long.

4.1.7.2 Thermoluminescence Reader

The automatic TLD reader of Harshaw model 5500 with TLD Shell software was used in the experiment. The reader uses hot nitrogen gas heating a closed loop feedback system and produces linearly ramped temperature up to 400°C. It can read up to 50 dosimeters in one loading [19].

4.1.8 Monte Carlo simulation

The Monte Carlo codes used for the accelerator head simulation and dose calculation in the phantom were BEAMnrc and DOSXYZnrc, respectively. Both codes were based on the EGSnrc code system. The EGSnrc system is a package for the Monte Carlo simulation of coupled electron-photon transport. Its current energy range of applicability is considered to be 1 keV to 10 GeV. For use with CT data, a separate program CTCREATE was used to convert the patient's CT data to the material types and mass densities. The software can be downloaded for free from the website <http://irs.inms.nrc.ca/software/egsnrc/>.

4.1.9 MATLAB and EXCEL software

In this study, MATLAB software version 7.7.0.2162 (R2008b) and Microsoft Office Excel 2007 were used for data analysis.

4.1.10 Personal Computer (PC)

The specification of the PC used for the simulation is Intel Pentium 4 with 2.8 GHz processor and 512 MB of RAM. The operating system is Linux Red hat enterprise 5.

4.2 Methods

The procedure of this research was divided into four major parts as

4.2.1 Treatment planning dose calculations

4.2.2 Monte Carlo Simulation

4.2.3 The determination of absolute dose for Monte Carlo simulation

4.2.4 TLDs measurements

4.2.1 Treatment planning dose calculations

We scanned the RANDO phantom by Phillips CT machine with 140 kVp protocols and applied the angiographic catheters to mark the reference point for treatment planning. Then the CT image data of RANDO phantom were transferred to the TPS (Pinnacle). The CT number for each pixel of the CT image was converted to the densities for use in dose calculation by using CT number to density curve as shown in Figure 4.6. This curve was generated by scan the Gammex 467 Tissue Characterization Phantom by the Phillips CT machine with 140 kVp protocol. The detail in process of generating of CT to density curve can be found in Ref. 9.

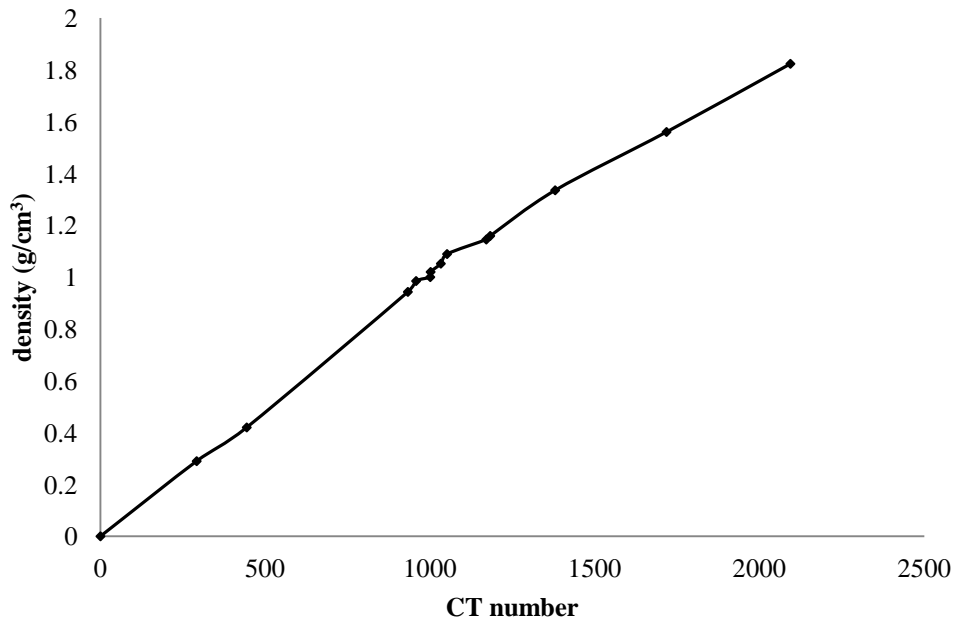
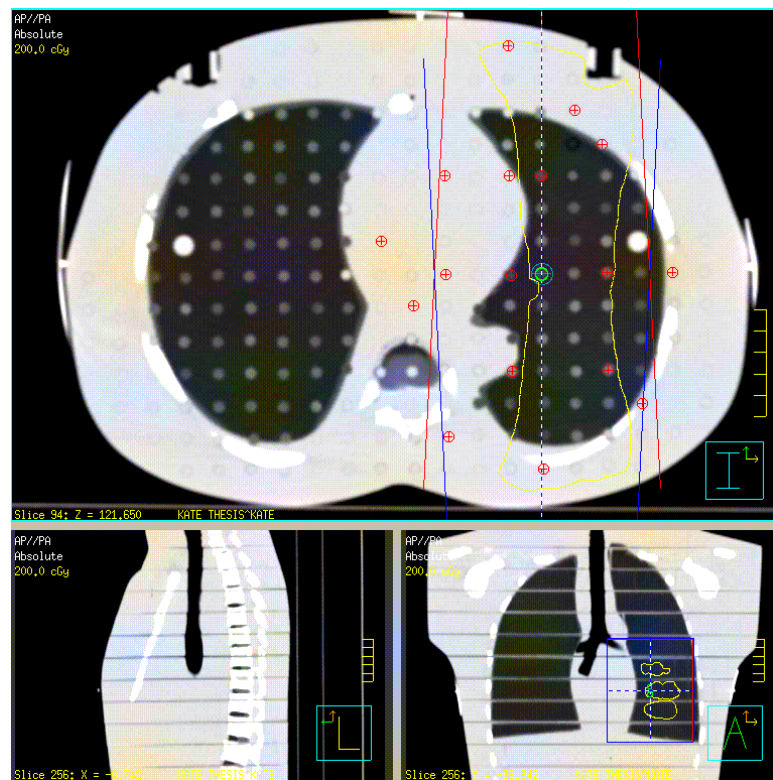
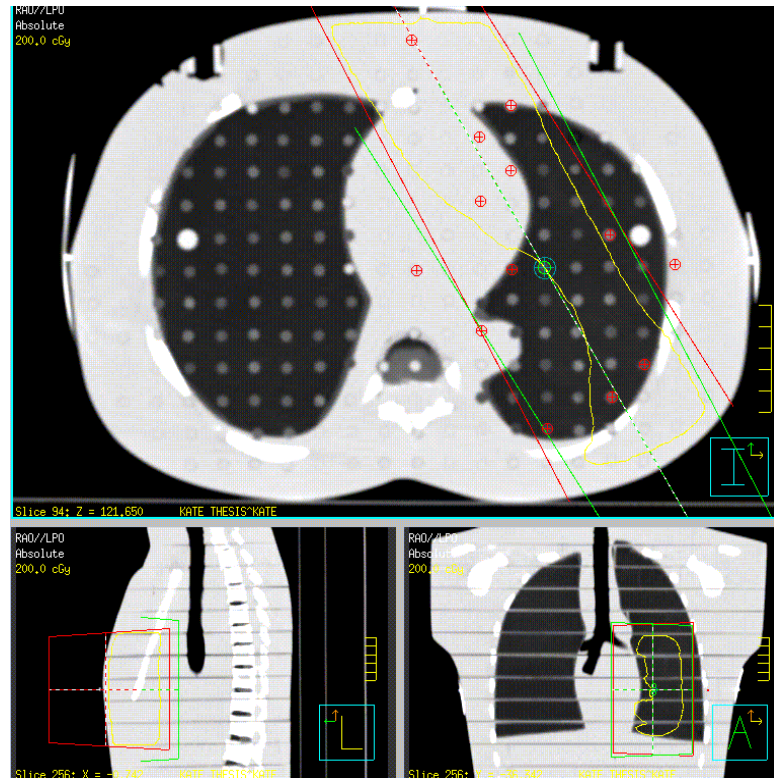


Figure 4.6 The CT number to density curve of 140 kVp of Phillips MX IDT 8000

The treatment planning was performed with 100 cm SAD technique. The investigated fields were $10 \times 12 \text{ cm}^2$ for AP-PA technique and $8 \times 15 \text{ cm}^2$ for RAO-LPO technique. These field sizes were chosen because those are frequently used in clinical situations. The calculation grid resolution size was 0.4 cm as the Pinnacle instruction for use [3] recommended that the fluence grid resolution should not be coarser than 0.4 cm and according to a study in verification of lung dose in an anthropomorphic phantom calculated by the collapsed cone convolution method [20], they examined the effect of grid resolution, tests were performed with resolutions ranging from 2 mm up to 1 cm in size. However, less than 2% variation in applied dose at depth was calculated for these changes in grid resolution. The placements of both fields were illustrated in Figure 4.7 (a) and (b), respectively. The phantom slices that involved in the treatment field are slice numbers 15 to 19 for AP-PA technique and 14 to 20 for RAO-LPO technique. For both techniques, we performed the calculated dose for slice number 16-18 at the points that located in the region recommended by the TG 53 (section 1.2). The plan summary and beam eye view were printed in order to delineate the treatment fields on the phantom surface.



(a)



(b)

Figure 4.7 Beam directions in two plans (a) AP-PA setup at beam central axis slice (b) RAO-LPO setup at beam central axis slice.

4.2.2 Monte Carlo Simulations

The Varian Clinac 2100C linear accelerator (Varian, Inc., Palo Alto, CA, USA) at the Department of Radiology, Ramathibodi Hospital was modelled by using the BEAMnrc code. The physical parameters of linac were provided by the manufacturer's specification. Since the output of the linac is known to be affected by the backscatter from the collimator jaws toward the monitor chamber, the backscatter corrections were considered in this study. As mentioned in the first chapter, a phase space file in BEAMnrc code can be scored on a specified plane [7]. In order to eliminate the need of correcting the output, we separated the linac simulation into two parts, A and B as shown in figure 4.8. Part A simulation is the simulation of the fixed components of the linac, a phase space files A was scored above the collimator jaws resulting in the dose accumulated in the monitor chamber due to the beam entering the chamber from above. This phase space was later used as a source for part B simulation, a phase space file B was scored under the collimator jaws resulting in the

dose accumulated in the monitor chamber due to the particles backscattered from the jaws. This method allows an accurate calculation of absolute dose, based on scoring the backscatter dose for every simulated field.

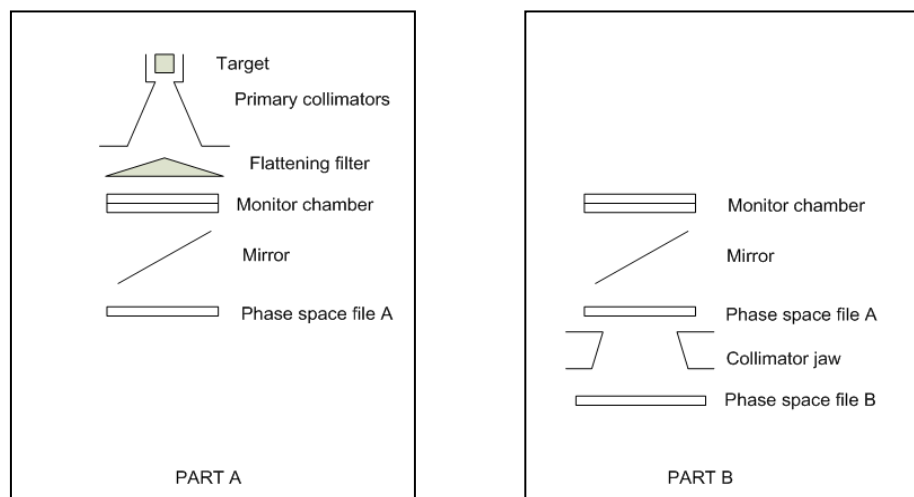


Figure 4.8 A schematic of the linac treatment head. Part A is the fixed components of linac and part B is the variable components.

For dose calculation in phantom, the same CT data set as used in the ADAC Pinnacle TPS was converted to a suitable format for DOSXYZnrc by using CTCREATE code. The information required to run CTCREATE code includes the CT format, the CT data file name, and voxel dimensions for the simulation phantom [8]. In this study, the voxel size of the phantom was set to $0.4 \times 0.4 \times 0.5 \text{ cm}^3$ in order to match that on the dose grid resolution of TPS. The density for a given voxel was assigned by the same CT number to density curve that used in the TPS (Figure 4.6).

For dose comparison, all dose calculated by TPS in section 4.2.1 were recalculated by using the Monte Carlo calculation. Because of the MC report the dose deposited in a region of a component module or in a phantom voxel as a relative dose, normalized by the number of electrons incident on the linac target [7,8], we have to develop the formalism for MC absolute dose calculation (see below).

4.2.3 The determination of absolute dose for Monte Carlo simulation

4.2.3.1 Derivation of the dose-MU equation [13]

As mentioned above, the MC output data are the dose in each calculation voxel per particle incident on the target. These characteristic of BEAMnrc and DOSXYZnrc code allow absolute dose result to be obtained.

Let us assume that a single filed MC simulation results in a normalized dose in the phantom, D_{xyz} , being deposited in a given voxel. By definition, this quantity represents the dose deposited in that phantom voxel as a result of one electron hitting the linac target. If N_e electrons are incident on the target, then the total absolute dose deposited in that voxel is

$$D_{xyz,abs} = D_{xyz} \cdot N_e \quad (1)$$

In order to introduce the number of monitor units in this equation, we have to relate it to the number of particles, N_e , through the dose accumulated at the same time in the monitor chamber. If one particle incident on the target leads to the accumulation of a dose D_{ch} in the monitor chamber, then the total absolute dose accumulated due to N_e particles is

$$D_{ch,abs} = D_{ch} \cdot N_e \quad (2)$$

On the other hand, this absolute dose can also be expressed as

$$D_{ch,abs} = D_{ch,abs}^{1MU} \cdot U \quad (3)$$

where $D_{ch,abs}^{1MU}$ is the absolute dose accumulated in the monitor chamber for one monitor unit

U is the number of monitor units

From equation (2) and (3), we have

$$N_e = \frac{D_{ch,abs}^{1MU}}{D_{ch}} \cdot U \quad (4)$$

Inserting equation (4) into (1), we obtain an equation for the absolute dose in any phantom:

$$D_{xyz,abs} = D_{xyz} \cdot \frac{D_{ch,abs}^{1MU}}{D_{ch}} \cdot U \quad (5)$$

The absolute dose $D_{ch,abs}^{1MU}$ is the constant that can be obtained under the standard calibration condition (same as the linac calibration condition [21]: dose at the machine isocenter, at the depth of maximum dose (d_{max}) with field size ($10 \times 10 \text{ cm}^2$). In practice, the measurement point is commonly placed at a depth of 10 cm in order to eliminate the effect of electron contamination. Then the tissue-maximum ratio (TMR) is used to calculate absorbed dose at d_{max} . Determination of absorbed dose under reference condition detail is in Appendix A. In order to match the simulated data with the measurement data, we scored dose in water phantom at depth of 10 cm.

We can now correlate the dose accumulated in the monitor chamber with the dose accumulated in a water phantom under standard calibration condition, and associate a corresponding number of monitor units with the monitor chamber dose. Let N_e^{1MU} be the number of electrons incident on the target for a photon beam calibration condition of 1 MU. With this condition, equation (2) becomes

$$D_{ch,abs}^{1MU} = D_{ch(10 \times 10)} \cdot N_e^{1MU} \quad (6)$$

and equation (1) is

$$D_{xyz,abs}^{cal} = D_{xyz}^{cal} \cdot N_e^{1MU} \quad (7)$$

then we got

$$D_{ch,abs}^{1MU} = D_{ch(10 \times 10)} \cdot \frac{D_{xyz,abs}^{cal}}{D_{xyz}^{cal}} \quad (8)$$

We can now express the absolute dose equation (5) as

$$D_{xyz,abs} = D_{xyz} \cdot \frac{D_{ch}(10 \times 10)}{D_{ch}} \cdot \frac{D_{xyz,abs}^{cal}}{D_{xyz}^{cal}} \cdot U \quad (9)$$

As we separated the dose in monitor chamber into dose from forward scatter and backscatter, we have final equation used for the MC absolute dose calculation.

$$D_{xyz,abs} = D_{xyz} \cdot \frac{(D_{ch}^{forward} + D_{ch}^{back}(10 \times 10))}{(D_{ch}^{forward} + D_{ch}^{back})} \cdot \frac{D_{xyz,abs}^{cal}}{D_{xyz}^{cal}} \cdot U \quad (10)$$

4.2.3.2 Verification of the dose-MU equation

To investigate the accuracy of the MC absolute dose calculation, the simulations were performed in water phantom for various field sizes and depths as listed in Table 4.1 and the results are compared with the measurement. The measurement of absolute dose and output data were performed by using cylindrical and plane parallel plate ionization chambers, respectively.

Table 4.1 Field sizes and depths used in the verification of the dose-MU equation.

Field size (cm x cm)	Depth (cm)
Square fields	
5×5, 10×10, 15×15, 20×20, 30×30	d _{max} , 5, 10, 20
Rectangular fields	
8×10, 6×20	d _{max} , 5, 10, 20
5×30, 30×5	d _{max} , 5, 10, 20

4.2.4 TLD measurement

4.2.4.1 TLD Calibration

(a) All TLDs (119 rods) were annealed at 400 °C for 1 hour and 100 °C for 2 hours to clear the remaining exposure in the TLDs.

(b) The TLDs were placed in the perspex phantom and irradiated by the gamma ray from the cobalt-60 machine with the exposure time for the dose of 2 Gy. Those TLDs were pre-read annealed at 100 °C for 10 minute before

being read in unit of nanocoulombs (nC) by the TLD reader (the individual charge of each TLD = Q_i).

(c) The Element Correction Coefficient (ECC_i) for each TLD was calculated by using the equation:

$$ECC_i = \frac{\bar{Q}}{Q_i} \quad (11)$$

where \bar{Q} is the average value of all TLD's charges (Q_i).

(d) From the ECC_i in (c), twelve TLDs (10% of all TLDs) that had the ECC_i value closest to 1 were chosen to use for the calibrations.

(e) The twelve dosimeters from (d) were irradiated and read with the same technique in (b). From the individual reading of each TLD (Q_i), the corrected charge integral (Q_{ci}) was calculated by following equation:

$$Q_{ci} = Q_i \times ECC_i \quad (12)$$

The average value of the Q_{ci} for the standard TLDs, \bar{Q}_c , was calculated and then the reader calibration factor (RCF) for the whole set of TLDs were determined by

$$RCF = \frac{\bar{Q}_c}{D} \quad (13)$$

where D is known dose radiation with 2 Gy.

(f) The rest of TLDs were calibrated by taking the same steps in (b), then we determined the individual element correction coefficients (ECC_{ci}) by using the equation:

$$ECC_{ci} = \frac{RCF \times L}{Q_i} \quad (14)$$

where L is a known radiation dose that was 2 Gy

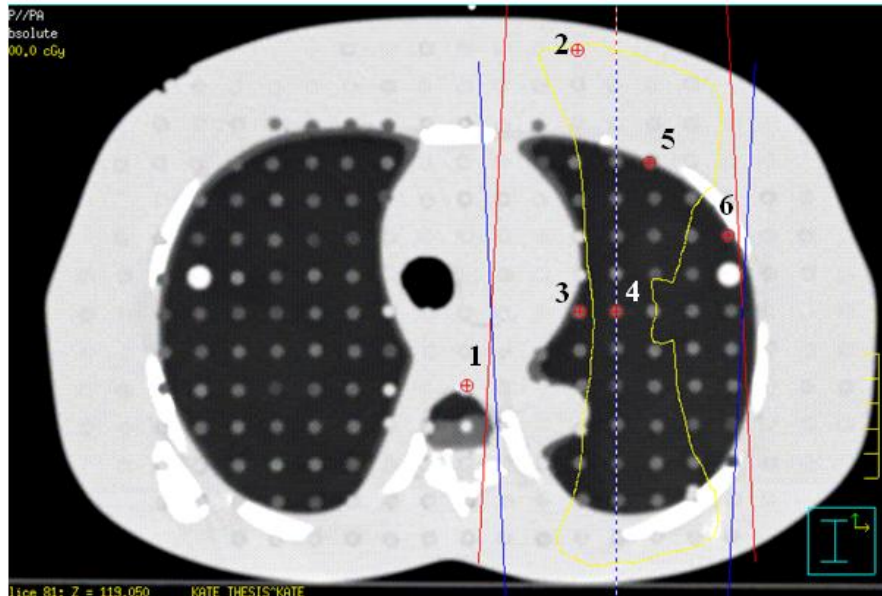
The ECC_{ci} for each TLD can be used to measure the unknown dose (D_u) of the radiation by using the equation.

$$D_u = \frac{Q_i \times ECC_i}{RCF} \quad (15)$$

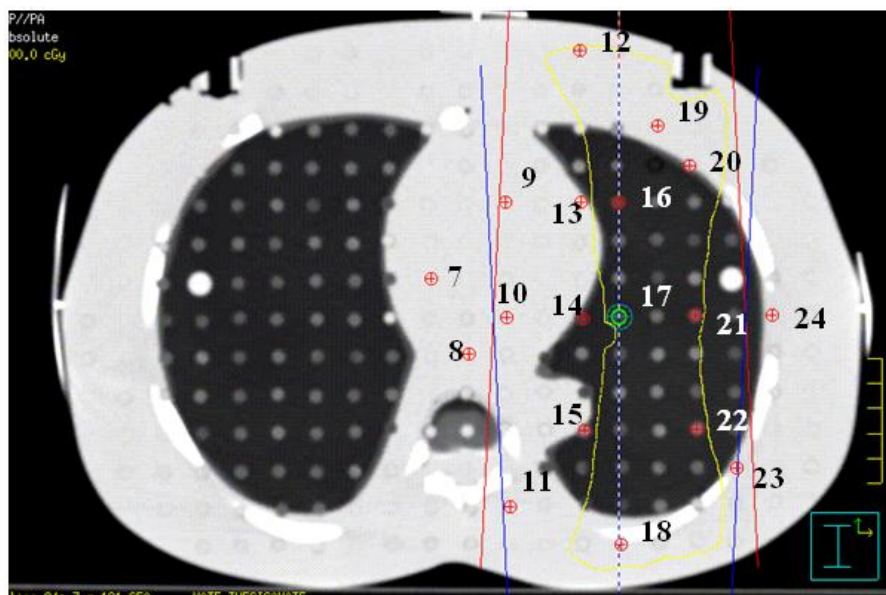
The linearity of all TLDs was checked by exposing those TLDs with the known dose of cobalt-60 gamma rays (0.25, 0.5, 1.0, 2.0 and 2.5 Gy). Then, the measured doses of the TLDs were plotted as a function of the irradiated values.

4.2.4.2 TLD measurement in Rando phantom

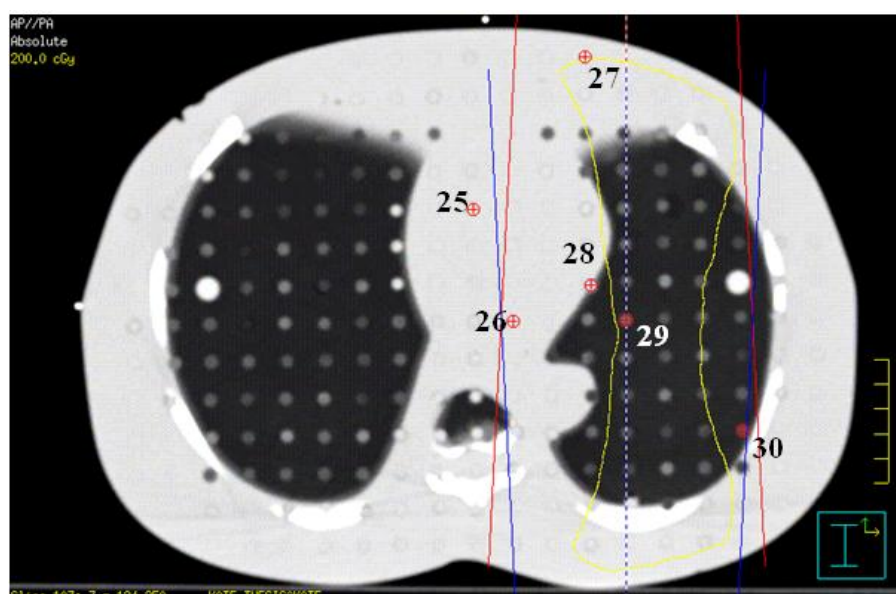
TLDs were loaded in the Rando phantom with the position illustrated in figure 4.9-4.10. Each point was inserted with the plug that held two TLD rods. Unused holes were filled with tissue equivalent plugs. Then dose deliver to the phantom was done with the same technique as used in both TPS and MC simulation. Repeat the above process three times in order to verify that the results are consistent.



(a) slice number 16

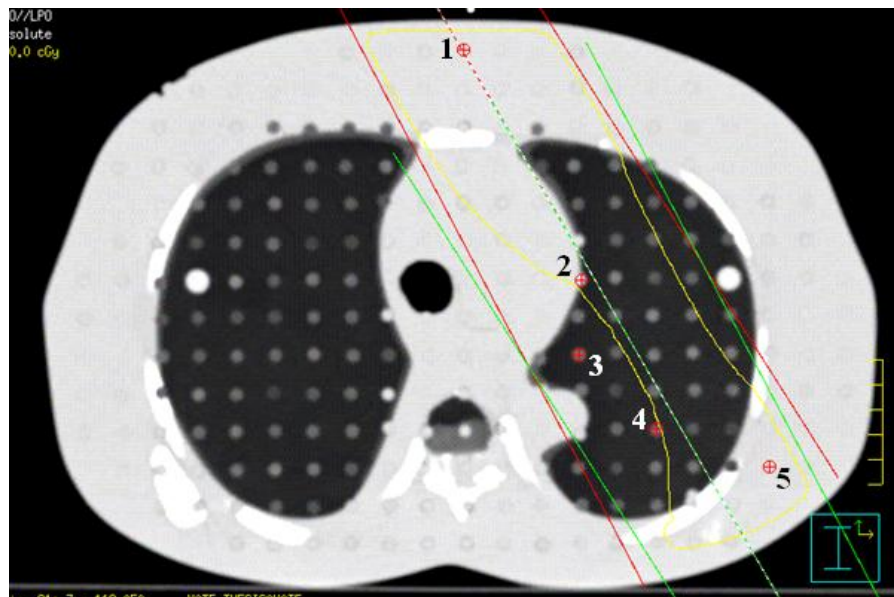


(b) slice number 17

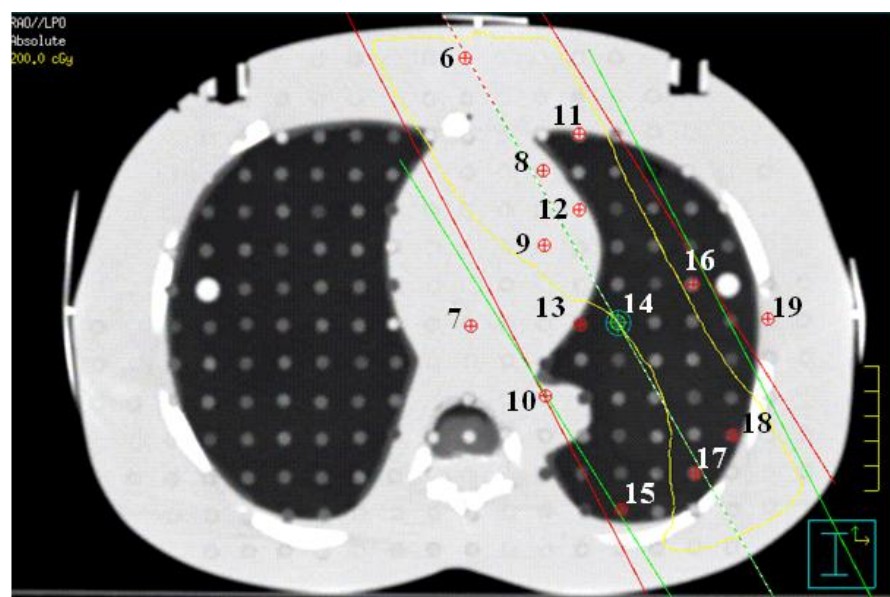


(c) slice number 18

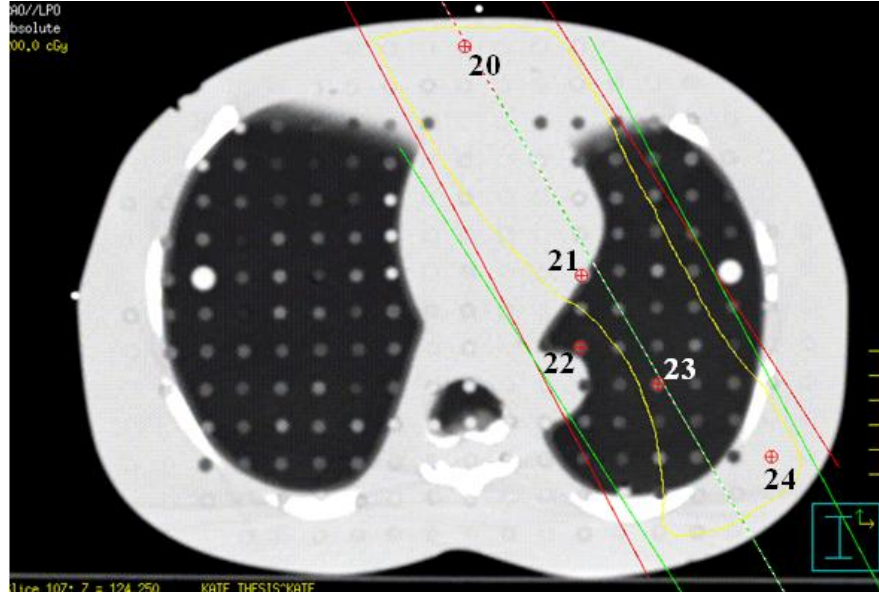
Figure 4.9 (a-c) Field directions for AP-PA setup and showing the measurement points for the slice numbers 16-18.



(a) slice number 16



(b) slice number 17



(c) slice number 18

Figure 4.10 (a-c) Field directions for RAO-LPO setup and showing the measurement points for the slice numbers 16-18.

The results of the absolute dose obtained from the Monte Carlo and treatment planning dose calculation were compared with the TLD measurement data. The percentage difference was calculated by equation (16).

$$\% \text{ difference} = \left(\frac{\text{Calculated dose} - \text{Measured dose}}{\text{Measured dose}} \right) \times 100 \quad (16)$$

Where; Calculated dose = point dose obtained from Monte Carlo and treatment planning dose calculations

Measured dose = point dose of TLD measurement

CHAPTER V

RESULTS AND DISCUSSIONS

5.1 The determination of absolute dose for Monte Carlo simulation

5.1.1 Absorbed dose measurement under reference conditions

The absorbed dose in water for 100 cm SAD at 10 cm depth, $D_{W,Q(d10)}$, measured under the reference condition were 0.7867 and 0.8397 cGy/MU for 6 and 10 MV respectively.

5.1.2 The dose-MU equation

From the simulations under the reference conditions, we obtained accumulated doses in the monitor chamber from both forward and backward photon beam ($D_{ch}^{forward}$ and D_{ch}^{back} (10×10)) as shown in table 5.1. The sum of these two quantities is the dose in the monitor chamber when one electron hits the target. This incident electron also causes a dose deposited at the calibration point (at the isocenter with 10 cm depth) in a water phantom (D_{xyz}^{cal}). The dose of $D_{xyz,abs}^{cal}$ was attributed to the calibration point. Thus, we obtain equation (17) and (18) for the MC absolute dose calculations for 6 and 10 MV, respectively.

Table 5.1 Relative dose obtained from MC simulations (normalized by the number of electrons incident on the target).

Simulated dose	6 MV	10 MV
$D_{ch,forward}$ (Gy/incident particle)	$2.261 \times 10^{-15} \pm 0.2\%$	$5.473 \times 10^{-15} \pm 0.1\%$
$D_{ch,back}$ (10×10) (Gy/incident particle)	$6.241 \times 10^{-17} \pm 1.3\%$	$1.748 \times 10^{-16} \pm 0.8\%$
$D_{cal,xyz}$ (Gy/incident particle)	$1.066 \times 10^{-16} \pm 0.9\%$	$2.611 \times 10^{-16} \pm 0.7\%$
$D_{cal,xyz,abs}$ (Gy)	0.00787	0.00839
$D_{1MU,ch,abs}$ (Gy)	0.1714	0.1817

$$D_{xyz,abs} = D_{xyz} \frac{0.1714 \text{ Gy}}{(2.261 \times 10^{-15} \text{ Gy} + D_{ch}^{back})} U \quad (17)$$

$$D_{xyz,abs} = D_{xyz} \frac{0.1817 \text{ Gy}}{(5.473 \times 10^{-15} \text{ Gy} + D_{ch}^{back})} U \quad (18)$$

5.1.3 Verification of the dose-MU equation

Table 5.2 (a-d) show the measured and calculated absolute doses in the water phantom of 6 and 10 MV photon beams for various rectangular field sizes and depths. The percentage difference was calculated by equation (19).

$$\% \text{ difference} = \left(\frac{\text{MC Simulation} - \text{Measurement}}{\text{Measurement}} \right) \times 100 \quad (19)$$

Where; MC Simulation = simulation data at the central axis of beam

Measurement = measurement data at the central axis of beam

Table 5.2 (a-d) The doses from MC calculation and measurement at (a) a depth of maximum dose (d_{max}) (b) 5 cm depth (c) 10 cm depth (d) 20 cm depth.

(a) a depth of maximum dose

FS	6 MV (1.5 cm)			10 MV (2.5 cm)		
	MC (Gy)	Meas (Gy)	%diff	MC (Gy)	Meas (Gy)	%diff
5x5	0.982	0.944	4.03	0.942	0.930	1.29
10x10	1.010	1.000	1.00	0.998	0.991	0.71
15x15	1.033	1.031	0.19	1.021	1.023	-0.20
20x20	1.050	1.051	-0.10	1.042	1.041	0.10
30x30	1.078	1.079	-0.09	1.053	1.069	-1.50
6x20	1.012	1.002	1.00	0.991	0.992	-0.10
8x10	1.009	0.993	1.61	0.988	0.983	0.51
5x30	1.009	0.999	1.00	0.986	0.988	-0.20
30x5	0.987	0.977	1.02	0.970	0.962	0.83

(b) at 5 cm depth.

FS	6 MV			10 MV		
	MC (Gy)	Meas (Gy)	%diff	MC (Gy)	Meas (Gy)	%diff
5x5	0.880	0.861	2.21	0.896	0.891	0.56
10x10	0.935	0.928	0.75	0.961	0.953	0.84
15x15	0.967	0.964	0.31	0.980	0.984	-0.41
20x20	0.992	0.986	0.61	1.002	1.004	-0.20
30x30	1.017	1.018	-0.10	1.027	1.033	-0.58
6x20	0.940	0.925	1.62	0.964	0.953	1.15
8x10	0.930	0.919	1.20	0.943	0.946	-0.32
5x30	0.933	0.921	1.30	0.949	0.947	0.21
30x5	0.908	0.900	0.89	0.929	0.925	0.43

(c) at 10 cm depth.

FS	6 MV			10 MV		
	MC (Gy)	Meas (Gy)	%diff	MC (Gy)	Meas (Gy)	%diff
5x5	0.718	0.705	1.84	0.773	0.764	1.18
10x10	0.787	0.785	0.25	0.84	0.836	0.48
15x15	0.831	0.830	0.12	0.879	0.876	0.34
20x20	0.861	0.859	0.23	0.900	0.899	0.11
30x30	0.905	0.899	0.67	0.928	0.933	-0.54
6x20	0.783	0.778	0.64	0.837	0.830	0.84
8x10	0.773	0.772	0.13	0.822	0.825	-0.36
5x30	0.768	0.77	-0.26	0.830	0.824	0.73
30x5	0.758	0.755	0.40	0.804	0.806	-0.25

(d) at 20 cm depth.

FS	6 MV			10 MV		
	MC (Gy)	Meas (Gy)	%diff	MC (Gy)	Meas (Gy)	%diff
5x5	0.464	0.459	1.09	0.550	0.546	0.73
10x10	0.527	0.532	-0.94	0.614	0.617	-0.49
15x15	0.579	0.581	-0.34	0.657	0.661	-0.61
20x20	0.610	0.617	-1.13	0.696	0.691	0.72
30x30	0.661	0.665	-0.60	0.729	0.734	-0.68
6x20	0.520	0.525	-0.95	0.611	0.611	0.00
8x10	0.513	0.518	-0.97	0.609	0.605	0.66
5x30	0.515	0.519	-0.77	0.602	0.605	-0.50
30x5	0.501	0.510	-1.76	0.594	0.593	0.17

The results show good agreement between the calculated and measured values with the percent difference of less than 2% for all measurements with the exception at the depth of maximum dose (d_{\max}) for the small field size of $5 \times 5 \text{ cm}^2$ with 6 MV that the difference was 4.03%. This may be because of the error of the simulation for the small field size with the shallow depth. In general, these results proved that our MC absolute dose equations, i.e. (17) and (18), have an acceptable accuracy to estimate the absolute dose for 6 and 10 MV photon beams with the field size of 5×5 to $30 \times 30 \text{ cm}^2$ and the depth of d_{\max} to 20 cm.

5.2 The comparison of doses in the chest Rando phantom between treatment planning dose calculation, Monte Carlo simulations and TLDs measurements

5.2.1 TLD Calibration

The ECC_i value of each TLD was shown in table 5.3. The value varied from 0.8391 to 1.0949. These variations were within the acceptable range (0.7-1.3) recommended in the manual [19].

The reader calibration factor (RCF) was 1.426×10^2 nC/Gy. Table 5.4 shows the calibration value of each TLD (ECC_{ci}). These values were ranged from 0.8400 to 1.0988.

Figure 5.1 shows that the absolute doses measured by the TLDs and as the function of irradiated known dose were linear with $R^2 = 0.9997$.

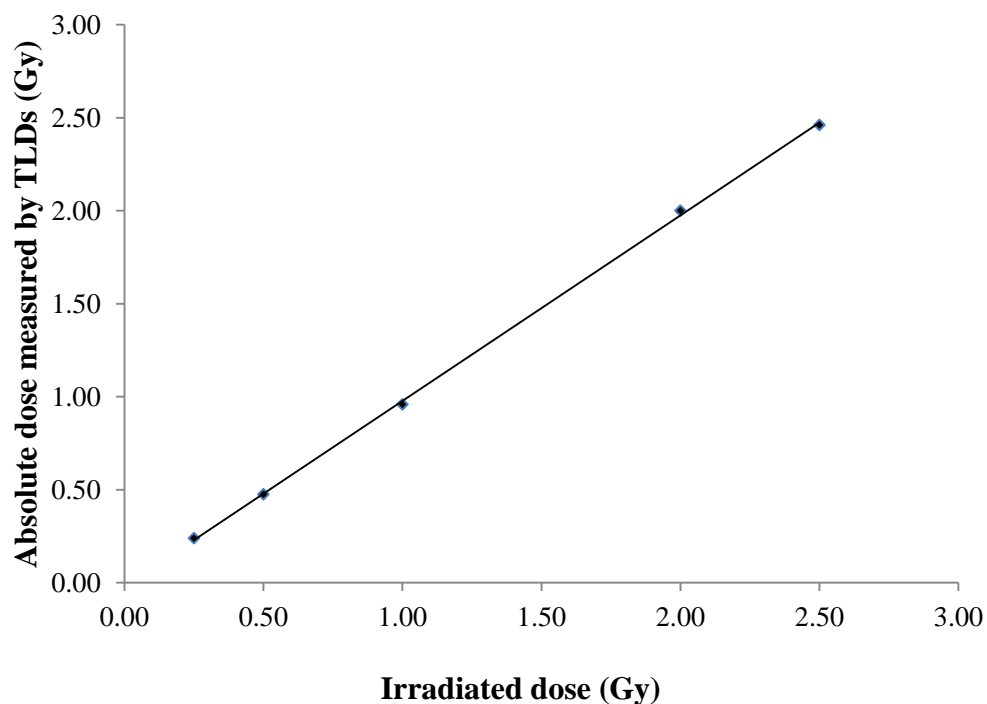


Figure 5.1 The linearity of the TLDs

Table 5.3 Individual element correction coefficient (ECC_i) value for each TLD

TLD No	ECC_i	TLD No	ECC_i	TLD No	ECC_i	TLD No	ECC_i
1	1.0189	31	0.9761	61	1.0339	91	0.9829
2	1.0308	32	0.9806	62	1.0243	92	1.0042
3*	1.0010	33	0.9716	63	0.9972*	93	0.9587
4	0.9889	34	1.0799	64	1.0059	94	0.9930
5	0.9647	35	1.0086	65	0.9951	95	1.0716
6	1.0199	36	0.9770	66	0.9941	96	0.9863
7	1.0090	37	1.0203	67	0.9334	97	0.9632
8	1.0180	38	1.0318	68	1.0202	98	1.0385
9	1.0407	39	1.0066	69	1.0235	99	0.9856
10	0.9689	40	1.0843	70	1.0090	100	1.0080
11	1.0176	41	0.9654	71	1.0529	101	0.9386
12*	1.0011	42	0.9640	72	0.9852	102	1.0021*
13	0.9951	43	0.9850	73	1.0168	103	1.0294
14	1.0449	44	0.9130	74	1.0239	104	0.9894
15	1.0199	45	0.9334	75	1.0482	105	0.9973*
16	0.9927	46	1.0282	76	0.9971*	106	0.9911
17*	0.9998	47	1.0934	77	1.0044	107	1.0036*
18	1.0536	48	1.0074	78	1.0308	108	1.0736
19	0.9678	49*	1.0007	79	0.9791	109	0.9749
20	1.0073	50	1.0397	80	1.0121	110	1.0119
21	0.9756	51	0.9784	81	0.9944	111	0.9434
22*	1.0037	52	0.9724	82	0.9852	112	1.0110
23	0.9271	53	1.0386	83	1.0433	113	0.8391
24	1.0042	54	1.0304	84	0.9990*	114	0.9105
25	0.9889	55	0.9447	85	1.0615	115	0.9794
26	1.0066	56*	1.0013	86	1.0338	116	0.9886
27	1.0236	57	0.9827	87	1.0473	117	1.0304
28	1.0145	58	1.0045	88	1.0550	118	0.9185
29	1.0949	59	1.0095	89	0.9855	119	0.9653
30	1.0074	60	0.9783	90	0.9825		

* The TLDs used for calibration

Table 5.4 The corrected individual element correction coefficient (ECC_{ci}) value for each TLD

TLD No	ECC_{ci}	TLD No	ECC_{ci}	TLD No	ECC_{ci}	TLD No	ECC_{ci}
1	1.0333	31	0.9750	61	1.0286	91	0.9652
2	1.0480	32	0.9735	62	1.0073	92	1.0002
3	1.0172	33	0.9686	63	0.9954	93	0.9634
4	0.9986	34	1.0835	64	1.0049	94	0.9922
5	0.9732	35	0.9978	65	0.9790	95	1.0848
6	1.0382	36	0.9695	66	0.9862	96	0.9927
7	1.0196	37	1.0207	67	0.9384	97	0.9512
8	1.0443	38	1.0187	68	0.9998	98	1.0331
9	1.0473	39	1.0091	69	1.0194	99	0.9770
10	0.9722	40	1.0786	70	1.0113	100	1.0034
11	1.0106	41	0.9571	71	1.0711	101	0.9307
12	1.0024	42	0.9669	72	0.9844	102	1.0007
13	0.9959	43	0.9826	73	1.0173	103	1.0303
14	1.0495	44	0.9070	74	1.0289	104	0.9775
15	1.0147	45	0.9367	75	1.0406	105	0.9896
16	0.9942	46	1.0420	76	0.9995	106	0.9750
17	1.0008	47	1.0870	77	1.0064	107	0.9981
18	1.0671	48	1.0268	78	1.0239	108	1.0650
19	0.9549	49	1.0015	79	0.9791	109	0.9814
20	1.0129	50	1.0326	80	1.0137	110	1.0231
21	0.9748	51	0.9860	81	1.0011	111	0.9523
22	0.9992	52	0.9685	82	1.0055	112	1.0345
23	0.9288	53	1.0528	83	1.0498	113	0.8400
24	1.0042	54	1.0383	84	1.0024	114	0.9177
25	0.9963	55	0.9440	85	1.0618	115	0.9775
26	0.9930	56	0.9975	86	1.0272	116	1.0007
27	1.0178	57	0.9696	87	1.0339	117	1.0384
28	1.0232	58	1.0122	88	1.0434	118	0.9281
29	1.0988	59	0.9933	89	0.9828	119	0.9735
30	0.9963	60	0.9747	90	0.9662		

5.2.2 The comparison of dose in the Rando phantom: AP-PA fields

Table 5.5 illustrates the absorbed doses with percent relative standard deviation (%RSD) measured by the TLDs in the RANDO phantom for 6 and 10 MV photon beam (all of TLD measurement data were shown in Appendix B). For 6 MV, there are 4 points that show the RSD with more than 3%. They were located at out of the beam and beam edge regions. The maximum value was 8.87% at the point no. 1 which was situated at the outside of beam area. The RSD of the 10 MV measured dose was high at point number 23 which was lie on beam edge with the value of 6.36%.

Table 5.6 and 5.7 present the percent difference of calculated dose from MC simulation and treatment planning dose calculation to the measured dose of 6 and 10 MV photon beams, respectively. The doses obtained from the Monte Carlo method were in better agreement with the measurement than that of the treatment planning system, especially within the inner beam region regardless of the heterogeneity. The large variations in MC dose calculation were found at the penumbra and outer beam region. The maximum difference between MC calculation and measurement was found at the point no.8.

Table 5.5 Absorbed doses in the RANDO phantom measured by the TLDs for AP-PA fields

point	6 MV		10 MV	
	Absored dose (Gy)	%SD	Absored dose (Gy)	%RSD
1	0.176	8.87	0.183	1.22
2	1.930	0.55	1.738	0.32
3	1.768	0.67	1.801	1.29
4	1.847	0.29	1.871	2.04
5	1.969	1.74	1.924	2.36
6	1.691	1.83	1.659	0.46
7	0.100	1.02	0.085	0.75
8	0.189	3.40	0.191	0.69
9	1.512	6.22	1.519	2.71
10	1.503	0.67	1.486	1.25
11	1.725	0.52	1.671	0.76
12	1.974	0.62	1.758	0.56
13	1.868	0.68	1.862	0.76
14	1.776	1.15	1.791	0.65
15	1.807	0.27	1.798	0.83
16	1.983	0.88	1.939	1.23
17	1.927	0.25	1.886	1.23
18	1.921	0.72	1.896	1.10
19	2.035	0.95	1.947	0.72
20	2.064	1.40	1.971	0.37
21	1.893	0.28	1.837	0.30
22	1.883	1.27	1.881	0.40
23	1.485	6.09	1.497	6.36
24	0.168	3.83	0.186	2.50
25	0.160	5.75	0.157	3.47
26	1.578	1.39	1.552	1.93
27	1.912	3.11	1.662	2.04
28	1.855	0.09	1.723	1.01
29	1.964	0.94	1.829	1.90
30	1.583	1.28	1.546	1.81

Table 5.6 Monte Carlo and Pinnacle dose calculation compared with measured TLD dose: 6 MV photon beam, AP-PA technique.

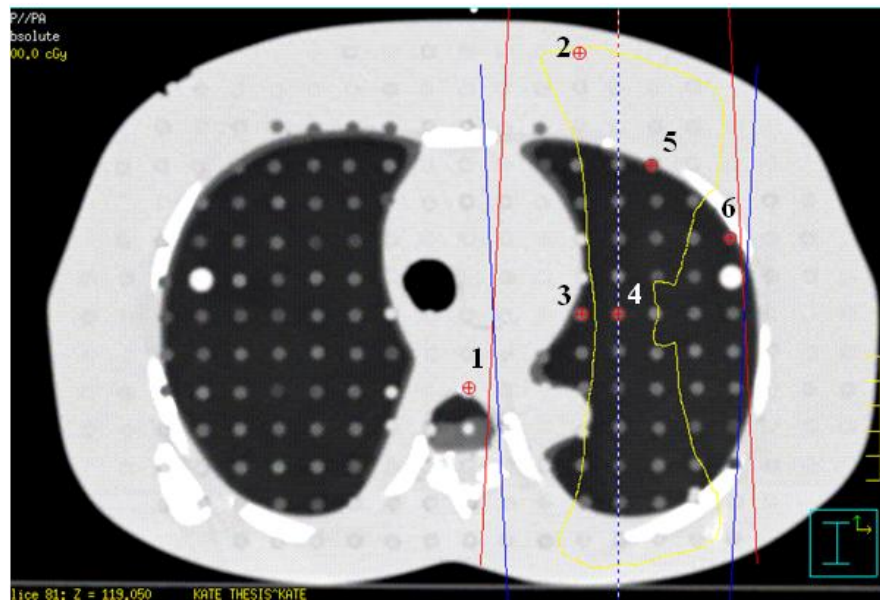
point	region	MC (Gy)	TPS (Gy)	MEA (Gy)	% diff	
					MC_Mea	TPS_Mea
1	OB	1.001	0.176	0.176	468.8	0.0
2	NS	2.088	2.053	1.930	8.2	6.4
3	IB: lung	1.914	1.938	1.768	8.3	9.6
4	IB: lung	1.948	2.007	1.847	5.5	8.7
5	IB: LT	1.994	2.076	1.969	1.3	5.4
6	PN, LB	1.845	1.723	1.691	9.1	1.9
7	OB	0.133	0.109	0.100	33.0	9.0
8	OB	1.123	0.191	0.189	494.2	1.1
9	PN	1.711	1.491	1.512	13.2	-1.4
10	PN	1.640	1.551	1.503	9.1	3.2
11	PN	1.828	1.579	1.725	6.0	-8.5
12	NS	2.031	2.038	1.974	2.9	3.2
13	IB: LT	1.897	1.945	1.868	1.6	4.1
14	IB: LT	1.855	1.900	1.776	4.4	7.0
15	IB: LT	1.896	1.944	1.807	4.9	7.6
16	IB: lung	1.973	2.033	1.983	-0.5	2.5
17	isocenter	1.950	2.004	1.927	1.2	4.0
18	IB: BT	2.034	2.117	1.921	5.9	10.2
19	IB: tissue	2.039	2.120	2.035	0.2	4.2
20	IB: LT	2.031	2.141	2.064	-1.6	3.7
21	IB: lung	1.990	2.020	1.893	5.1	6.7
22	IB: lung	2.034	2.041	1.883	8.0	8.4
23	PN	2.034	1.380	1.485	37.0	-7.1
24	OB: LT	0.460	0.193	0.168	173.8	14.9
25	OB	0.479	0.166	0.160	199.4	3.8
26	PN	1.655	1.556	1.578	4.9	-1.4
27	NS	2.055	1.944	1.912	7.5	1.7
28	IB: LT	1.823	1.907	1.855	-1.7	2.8
29	IB: lung	1.953	2.012	1.964	-0.6	2.4
30	PN, LB	2.007	1.536	1.583	26.8	-3.0

*The abbreviations used in table 5.6-5.7 and 5.9-5.10:

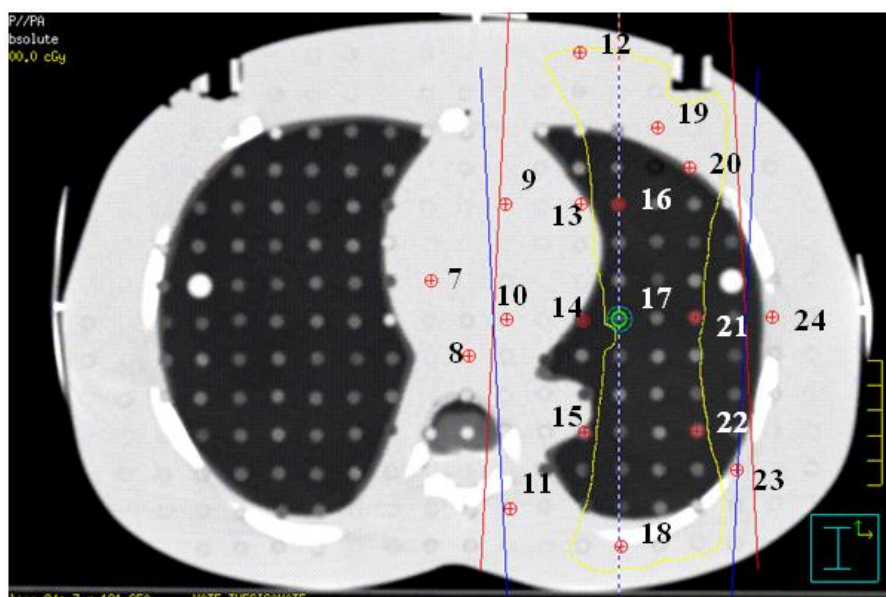
- NS = Near surface
- PN = Penumbra
- OB = Outer beam region
- IB = Inner beam region
- LT = Lung-tissue interface
- BT = Bone-tissue interface
- LB= Lung-bone interface

Table 5.7 Monte Carlo and Pinnacle dose calculation compared with measured TLD dose: 10 MV photon beam, AP-PA technique.

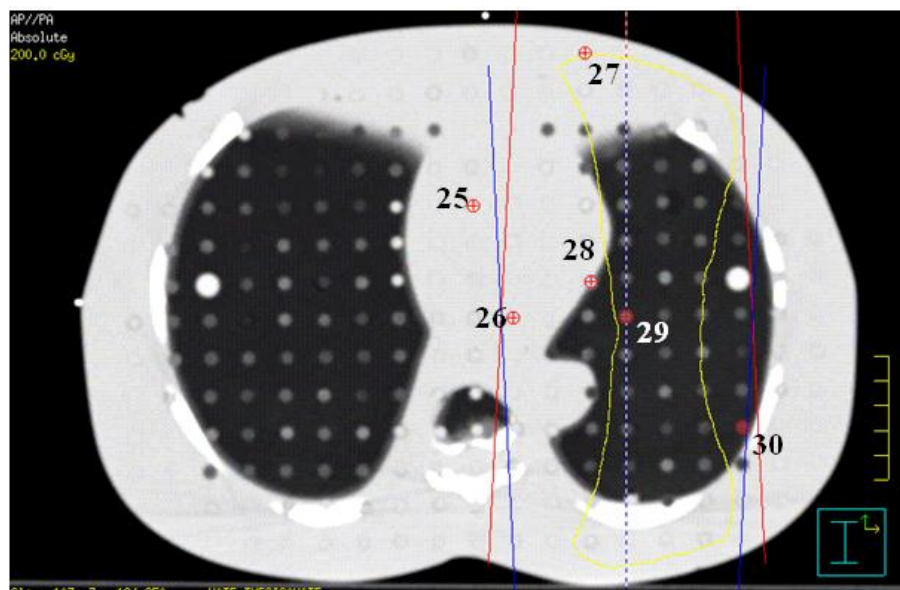
point	region	MC (Gy)	TPS (Gy)	MEA (Gy)	% diff	
					MC_Mea	TPS_Mea
1	OB	0.905	0.152	0.183	394.5	-16.9
2	NS	1.990	1.846	1.738	14.5	6.2
3	IB: lung	1.865	1.942	1.801	3.6	7.8
4	IB: lung	1.895	1.992	1.871	1.3	6.5
5	IB: LT	1.927	2.058	1.924	0.2	7.0
6	PN, LB	1.816	1.691	1.659	9.5	1.9
7	OB	0.121	0.095	0.085	42.4	11.8
8	OB	0.977	0.164	0.191	411.5	-14.1
9	PN	1.733	1.508	1.519	14.1	-0.7
10	PN	1.745	1.557	1.486	17.4	4.8
11	PN	1.824	1.536	1.671	9.2	-8.1
12	NS	1.965	1.861	1.758	11.8	5.9
13	IB: LT	1.862	1.960	1.862	0.0	5.3
14	IB: LT	1.843	1.922	1.791	2.9	7.3
15	IB: LT	1.896	1.955	1.798	5.5	8.7
16	IB: lung	1.945	2.032	1.939	0.3	4.8
17	isocenter	1.917	2.001	1.886	1.6	6.1
18	IB: BT	1.887	2.026	1.896	-0.5	6.9
19	IB: tissue	1.980	2.086	1.947	1.7	7.1
20	IB: LT	1.968	2.094	1.971	-0.2	6.2
21	IB: lung	1.911	1.967	1.837	4.0	7.1
22	IB: lung	1.981	1.993	1.881	5.3	6.0
23	PN	1.945	1.391	1.497	29.9	-7.1
24	OB: LT	0.423	0.195	0.186	127.4	4.8
25	OB	0.454	0.141	0.157	189.2	-10.2
26	PN	1.654	1.551	1.552	6.6	-0.1
27	NS	1.929	1.725	1.662	16.1	3.8
28	IB: LT	1.810	1.921	1.723	5.0	11.5
29	IB: lung	1.907	1.996	1.829	4.3	9.1
30	PN, LB	1.945	1.466	1.546	25.8	-5.2



(a) slice number 16



(b) slice number 17



(c) slice number 18

Figure 5.2 (a-c) Field directions for AP-PA setup and the numbers indicate the points of dose investigation for slice number 16-18.

5.2.3 The comparison of dose in a Rando phantom: RAO-LPO fields

Table 5.8 shows the absorbed dose with the %RSD at 30 points for 6 and 10 MV. Only one point shows the RSD with more than 3%, which is no.19 that had 4.74 %RSD. This point located at outside of the beam area.

The comparison of absolute dose from the calculations (Monte Carlo and TPS) and TLD measurements was showed in table 5.9-5.10 for 6 and 10 MV, respectively. In the inner beam region, the MC dose calculation gave more accurate results than Pinnacle calculation compared to the experimental data for both energies. However, we found the large deviation between the MC calculation and measurement in the penumbra and the outer beam regions. The maximum difference was found at point no.19 which located at out of beam region for both energies.

Table 5.8 Absorbed doses in the RANDO phantom measured by the TLDs for RAO-LPO fields

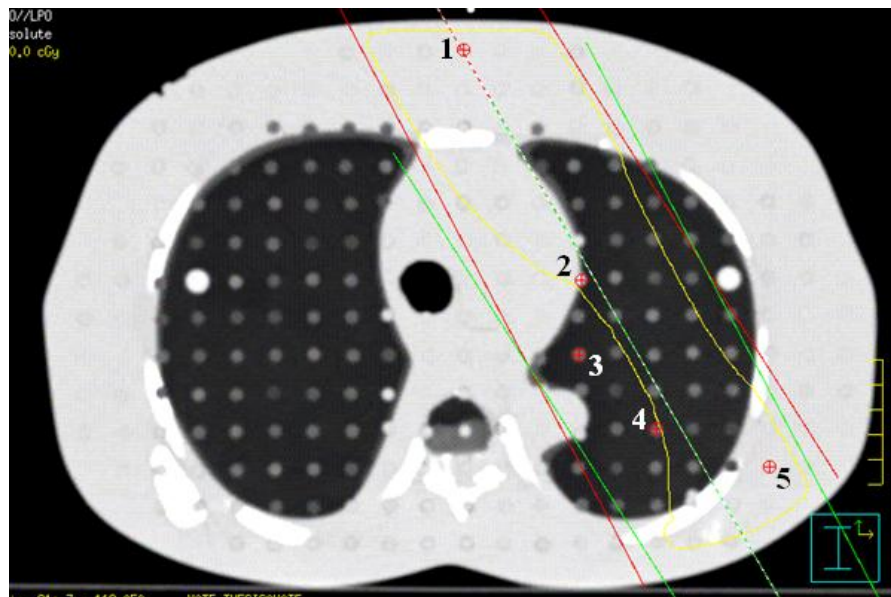
point	6 MV		10 MV	
	Absored dose (Gy)	%SD	Absored dose (Gy)	%RSD
1	2.342	0.82	2.086	0.37
2	1.877	0.78	1.868	0.95
3	1.805	1.19	1.800	2.66
4	1.836	0.78	1.873	1.98
5	2.143	0.99	2.078	0.71
6	2.357	0.70	2.137	0.47
7	0.186	0.67	0.165	0.57
8	2.048	0.84	2.000	1.30
9	1.880	0.56	1.839	0.60
10	1.438	1.48	1.309	0.25
11	2.206	0.52	2.100	3.94
12	2.065	1.01	2.032	1.52
13	1.923	0.71	1.905	0.56
14	1.867	1.10	1.868	0.68
15	1.625	0.97	1.537	1.91
16	1.779	1.79	1.700	2.77
17	1.921	0.67	1.881	2.39
18	2.067	0.52	2.060	1.96
19	0.167	4.74	0.175	2.38
20	2.453	1.58	2.083	0.71
21	1.973	1.47	1.892	1.22
22	1.824	1.81	1.796	1.05
23	1.908	2.03	1.871	2.03
24	2.150	3.39	2.010	1.42

Table 5.9 Monte Carlo and Pinnacle dose calculation compared with measured TLD dose: 6 MV photon beam, RAO-LPO technique.

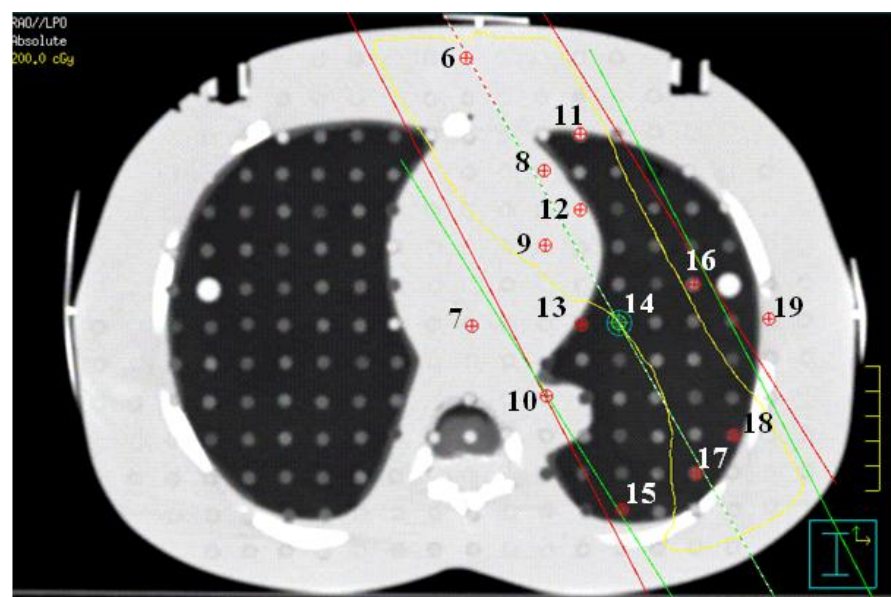
point	region	MC	TPS	MEA	% diff	
		(Gy)	(Gy)	(Gy)	MC_Mea	TPS_Mea
1	NS	2.322	2.463	2.342	-0.9	5.2
2	IB: LT	1.978	2.020	1.877	5.4	7.6
3	IB: lung	1.848	1.917	1.805	2.4	6.2
4	IB: lung	1.983	1.991	1.836	8.0	8.4
5	IB: tissue	2.170	2.216	2.143	1.3	3.4
6	NS	2.335	2.399	2.357	-0.9	1.8
7	OB	1.802	0.192	0.186	868.8	3.2
8	IB: tissue	2.170	2.185	2.048	6.0	6.7
9	IB: tissue	1.998	2.060	1.880	6.3	9.6
10	PN	1.836	0.953	1.438	27.7	-33.7
11	IB: LT	2.284	2.293	2.206	3.5	3.9
12	IB: LT	2.152	2.153	2.065	4.2	4.3
13	IB: LT	1.958	1.969	1.923	1.8	2.4
14	isocenter	2.008	2.000	1.867	7.6	7.1
15	PN	1.929	1.354	1.625	18.7	-16.7
16	IB: lung	2.181	1.879	1.779	22.6	5.6
17	IB: lung	2.074	2.027	1.921	8.0	5.5
18	IB: LT	2.150	2.151	2.067	4.0	4.1
19	OB	2.137	0.190	0.167	1179.6	13.8
20	NS	2.194	2.456	2.453	-10.6	0.1
21	IB: LT	1.977	2.048	1.973	0.2	3.8
22	IB: LT	1.879	1.950	1.824	3.0	6.9
23	IB: lung	2.000	2.024	1.908	4.8	6.1
24	IB: tissue	1.949	2.244	2.150	-9.3	4.4

Table 5.10 Monte Carlo and Pinnacle dose calculation compared with measured TLD dose: 10 MV photon beam, RAO-LPO technique.

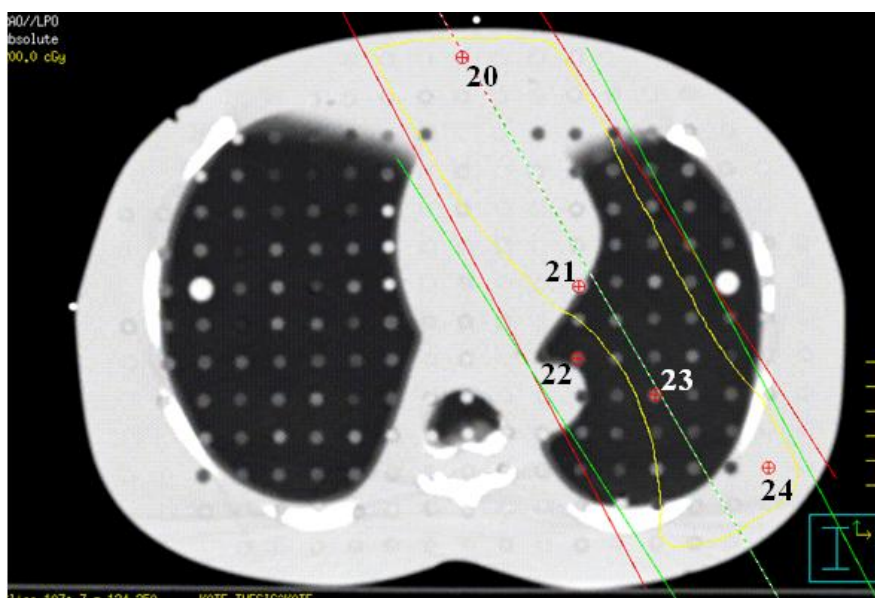
point	region	MC	TPS	MEA	% diff	
		(Gy)	(Gy)	(Gy)	MC_Mea	TPS_Mea
1	NS	2.035	2.180	2.086	-2.4	4.5
2	IB: LT	1.891	2.011	1.868	1.2	7.7
3	IB: lung	1.811	1.915	1.800	0.6	6.4
4	IB: lung	1.904	1.991	1.873	1.7	6.3
5	IB: tissue	1.960	2.148	2.078	-5.7	3.4
6	NS	2.051	2.143	2.137	-4.0	0.3
7	OB	1.829	0.164	0.165	1008.5	-0.6
8	IB: tissue	2.130	2.141	2.000	6.5	7.1
9	IB: tissue	1.969	2.045	1.839	7.1	11.2
10	PN	1.825	0.946	1.309	39.4	-27.7
11	IB: LT	2.186	2.197	2.100	4.1	4.6
12	IB: LT	2.095	2.112	2.032	3.1	3.9
13	IB: LT	1.918	1.969	1.905	0.7	3.4
14	isocenter	1.996	1.999	1.868	6.9	7.0
15	PN	1.900	1.324	1.537	23.6	-13.9
16	IB: lung	2.098	1.727	1.700	23.4	1.6
17	IB: lung	2.013	2.026	1.881	7.0	7.7
18	IB: LT	2.122	2.107	2.060	3.0	2.3
19	OB	2.031	0.178	0.175	1060.6	1.7
20	NS	1.866	2.178	2.083	-10.4	4.6
21	IB: LT	1.862	2.028	1.892	-1.6	7.2
22	IB: LT	1.838	1.944	1.796	2.3	8.2
23	IB: lung	1.875	2.014	1.871	0.2	7.6
24	IB: tissue	1.625	2.141	2.010	-19.2	6.5



(a) slice number 16



(b) slice number 17



(c) slice number 18

Figure 5.3 (a-c) Field directions for RAO-LPO setup and the numbers indicate the points of dose investigation for slice number 16-18.

The results of point dose comparison show good agreement between MC and measurement in the inner beam region for both inhomogeneous and interface location but some significant dose differences in MC dose calculation was found at the outer beam and penumbra regions for both techniques and energies. The cause of disagreement may be likely due to the inaccurate model of the beam parameters in MC simulation in those regions which have small dose or high gradient. So the disagreements might be improved by adding more parameters matching for the out of beam data in the beam model. According to the study of Omar Chibani on the Monte Carlo modeling of megavoltage photon beams, additional tuning beam parameters such as the beam radius and the angular divergence of primary electron beam were suggested for a better modeling [22].

Unfortunately, the calculation time of MC method is quite time-consuming since we used the phase space file as a source of the beam information. The computation time for Part A simulation (fixed components of linac) was 20-24 hr on a Pentium 4 with 2.8 GHz processor for 0.5-1 billion particle histories. But it was demanded for only once time. Part B simulation (variable components) took 5 min - 3 hr of CPU time on a Pentium 4 with 2.8 GHz processor. Using an alternative beam

source model would significantly save the calculation time in the treatment head simulation to achieve the same level of precision [23].

CHAPTER VI

CONCLUSIONS

The first aim of this study was to obtain the equations described the absolute dose from the Monte Carlo simulations of the 6 and 10 MV photon beams delivered from the medical linear accelerator (Varian Clinac 2100C) installed at Ramathibodi Hospital. The second aim was to compare the computed doses (the Pinnacle Treatment Planning System and MC calculations) in various locations within a chest Rando phantom to the measured doses obtained by TLDs.

In this study, the BEAMnrc code was used to generate the radiation beam specific data and the DOSXYZnrc code was used to simulate the absorbed doses in the phantom. Since the output data of Monte Carlo simulation are the dose in each calculation voxel per incident particle, we have obtained the parameters in the equation used for calculating the absolute dose for the Monte Carlo simulation based on the previous study [12] to fit our machine. The investigation of this equation were performed on the nine fields with the sizes of 5x5, 10x10, 15x15, 20x20, 30x30, 6x20, 8x10, 5x30 and 30x5 cm², at 4 depths (d_{\max} , 5, 10 and 20 cm) for 100-cm SAD technique. The results of absolute dose in the water phantom show good agreement between Monte Carlo calculation and measurement with the percent difference of less than 2% in all cases, except for the smallest field size (5x5) of the 6 MV beam. It proved that our equations have acceptable accuracy to calculate the absolute dose from the MC simulation.

For the comparison of dose in the Rando phantom, the absolute doses in different locations were determined by TLD measurement, treatment planning system (CCC algorithm), and Monte Carlo method. Typically, the results show that the doses obtained from the Monte Carlo method are in better agreement with the measurement than that of the treatment planning system, especially within the inner beam region regardless of the heterogeneity. The treatment plan gives the large overdose at the interface locations in the inner beam region. The same result was reported by Joseph

and Alvis [10]. The large deviation between the absolute dose obtained from Monte Carlo and measurement in the outer beam and beam edge regions are unfortunately observed. In these regions, the dose is generally quite small and rarely considered in the clinical use or changes rapidly. The disagreement might be the cause of inaccurate of the beam model in the MC beam simulation since the dose data in those regions had not been included during the beam-parameter findings. Therefore, better tuning of the beam parameters may be necessary for better MC absolute dose calculation. Additional beam parameters such as the beam radius and the angular divergence of the primary electron beam may be needed for a better beam model.

The dose calculation using the MC simulation is generally quite time-consuming not only because of the event-by-event tracking but also the reading of the phase space file for each beam particle. It takes much more time than the commercial treatment planning system in which the accuracy is somewhat less. This may be one of the reasons why the use of MC dose calculation for dose verification is impractical. Using an alternative beam source as well as a faster computer would help shorten the total calculation time.

REFERENCES

1. AAPM report No.85 Tissue inhomogeneity corrections for Megavoltage Photon Beam. Task Group No. 65 of the Radiation Therapy Committee of the American Association of Physicists in Medicine. 2004
2. Podgorsak E B, Technical Editor. Radiation oncology physics: a handbook for Teachers and students. INTERNATIONAL ATOMIC ENERGY AGENCY VIENNA, 2005.P 497
3. Radiation oncology System. Pinnacle3 Physics Instruction for use Release 7.4, Philips Medical System Inc., USA, 2004.
4. Fraass B, Doppke K, Hunt M, Kutcher G, Starkschall G, Stern R, et al. American Association of Physicists in Medicine Radiation Therapy Committee Task Group 53: quality assurance for clinical radiotherapy treatment planning. Med Phy 1998;25:1773-1829
5. Van Dyk J, Barnett RB, Cygler JE, Ghragge PC. Commissioning and Quality assurance of treatment planning computer. Int J Radiat Oncol Bio Phys 1993; 26:261-273.
6. Ma C M, Mok E, Kapur A, Pawlicki T, Findley D, Forster K, et al. Clinical implementation of a Monte Carlo treatment planning system. Med Phy 1999;26(10):2133-2143
7. Rogers DWO, Walters B, Kawrakow I. BEAMnrc Users Manual. NRCC Report PIRS-0509(A)revI, 2005
8. Walters BRB, Kawrakow I, Rogers DWO. DOSXYZnrc Users Manual. NRCC Report PIRS-794revB, 2006
9. Suchart Changmanee. Dosimetric verification of a treatment planning system for photo external beam therapy of Ramathibodi Hospital. [thesis]. Bangkok: Mahidol University; 2006

10. Carrasco P, Jornet N, Duch M A, Weber L, Ginjaume M, Eudaldo T, et al. Comparison of dose calculation algorithms in phantoms with lung equivalent heterogeneities under conditions of lateral electronic disequilibrium. *Med. Phys.* 2004;31(10) 2899-2911
11. Joseph R. Butts and Foster A E. Comparison of commercially available three-dimensional treatment planning algorithms for monitor unit calculations in the presence of heterogeneities. *JACMP* Vol 2, No 1 (2001)
12. Wyatt M, Corredor C, Tamimi M and Miller L F. Comparison of treatment planning dose calculations with measurements and Monte Carlo calculations in a Rando phantom. *Radiat Prot Dosimetry* (2005) 116 (1-4): 461-465.
13. Popescu I A, Shaw C P, Zavgorodni S F and Beckham W A. Absolute dose calculations for Monte Carlo simulations of radiotherapy beams *Phys. Med. Biol.* 50 (2005) 3375–3392
14. http://www.ibadosimetry.com/sites/default/files/ressources/DOSE_1_01.pdf
15. <http://scanditronix-wellhofer.com/WPID.830.0.html>
16. Philips medical system. Computed Tomography Mx8000 IDT version 3.1 user guides, Philips Medical Systems Inc., USA, 2004.
17. <http://www.medimagingsales.com/medical-imaging-equipment/ct/philips/philips-marconi-mx8000-idt-16-ct>
18. <http://www.radpro-int.com/accessories/phantoms/rsd/index.php>
19. Harshaw BICRON. Automatrix TLD Reader User's Manual, Saint-Gobain/Norton Industrial Ceramics Co., Ohio, 1993.
20. Martin J B, Rebecca E, Tsang C, Peter K N, Michael S, Kim Y Q, et al. Verification of lung dose in an anthropomorphic phantom calculated by the collapsed cone convolution method. *Phys. Med. Biol.* 45 (2000) N143–N149.
21. International Atomic energy Agency, Technical Report Series No.398: Absorbed dose determination in external beam radiotherapy. Vienna:2000

22. Omar C, Belal M, Charlie M. On Monte Carlo modeling of megavoltage photon beams: A revisited study on the sensitivity of beam parameters. Med. Phys. 2010;38(1) 188-201
23. C.-M. Ma and D. W. O. Rogers. BEAMDP Users Manual. NRC Report PIRS 509c, 1995.

APPENDICES

APPENDIX A

Absorbed dose measurement under reference conditions [21]

The absorbed dose at 10 cm depth for 10x10 cm² field size in the water phantom was determined under the reference conditions recommended by the IAEA TRS 398. The absorbed dose at 10 cm depth for 10x10 cm² field size was calculated by the equation (1).

$$D_{W,Q(Zref)} = M_Q N_{D,W,Q_0} k_{Q,Q_0} \quad (1)$$

Where M_Q is the corrected electrometer reading

N_{D,W,Q_0} is the calibration factor of absorbed dose to water for dosimeter at the reference quality Q_0

k_{Q,Q_0} is a chamber-specific factor which corrects for the difference between the reference beam quality Q_0 and the actual quality Q .

The reading M_Q can be calculated from the following equation:

$$M_Q = M_1 \cdot k_{pol} \cdot k_{TP} \cdot k_{elec} \cdot k_S \quad (2)$$

where M_1 is the electrometer reading using the normal operating bias voltage.

k_{pol} is the factor to correct the response of an ionization chamber for the effect of a change in polarity of the polarizing voltage applied to the chamber. The polarity effect can be derived from the equation:

$$k_{pol} = \frac{|M_+| + |M_-|}{2M} \quad (3)$$

Where M_+ and M_- are the electrometer readings obtained at positive and negative polarity, respectively, and M is the electrometer reading with the polarity used routinely (positive or negative)

k_{TP} is temperature and pressure correction factor determined by

$$k_{TP} = \frac{(273.2 + T)}{(273.2 + T_0)} \frac{P_0}{P} \quad (4)$$

where T and P are temperature and the air pressure in the chamber cavity during measurement.

T_0 and P_0 are the reference temperature and air pressure (20°C and 101.3 kPa)

k_{elec} is the calibration factor of an electrometer when the ionization chamber and electrometer are calibrated separately

k_S is the factor to correct the recombination effect. For the pulsed beam, the k_S can be derived by using from

$$k_S = a_0 + a_1 \left(\frac{M_1}{M_2} \right) + a_2 \left(\frac{M_1}{M_2} \right)^2 \quad (5)$$

where a_0 , a_1 and a_2 are the constant values given in Table 4.VII of the TRS 398. [398]

The measurement was made by the Farmer type chamber FC 65-G at the voltage of 300, -300 and 100 V for polarity effect correction and recombination effect correction. In each voltage, the readings were repeated at least five times or until the values were stable, then each average value was corrected for temperature and pressure.

APPENDIX B

All of TLDs measurement data with the percent relative standard deviation (%RSD) in the chest Rando phantom for 6 and 10 MV photon beam energy were shown in table B-1 to B-4. The relative standard deviation (RSD) is useful for comparing the uncertainty between different measurements of varying absolute magnitude. The RSD is calculated from the standard deviation, s , and is commonly expressed as percentage (%).

$$\%RSD = \left(\frac{S}{\bar{X}} \right) \times 100\% \quad (6)$$

Table B-1 TLDs measurement data for AP-PA fields: 6 MV.

Point	1 st Reading	2 nd Reading	3 rd Reading	Average	% RSD
1	16.07	19.19	17.55	17.60	8.87
2	192.23	194.21	192.54	192.99	0.55
3	175.44	177.28	177.64	176.79	0.67
4	184.31	184.59	185.33	184.74	0.29
5	199.66	193.08	198.00	196.91	1.74
6	167.28	167.36	172.67	169.10	1.83
7	9.81	10.40	9.81	10.00	3.40
8	17.98	20.20	18.44	18.87	6.22
9	150.15	151.20	152.16	151.17	0.67
10	150.47	150.95	149.41	150.28	0.52
11	173.04	173.15	171.26	172.48	0.62
12	198.92	196.71	196.50	197.37	0.68
13	188.30	187.75	184.34	186.80	1.15
14	178.02	177.65	177.06	177.58	0.27
15	179.86	179.78	182.56	180.73	0.88
16	197.82	198.80	198.21	198.28	0.25
17	193.68	193.98	190.42	192.69	1.02
18	190.56	192.75	193.12	192.14	0.72
19	203.25	205.61	201.77	203.54	0.95
20	208.31	207.79	203.08	206.39	1.40
21	189.86	189.37	188.80	189.34	0.28
22	186.84	186.99	191.06	188.29	1.27
23	158.25	140.40	146.84	148.50	6.09
24	17.36	16.10	16.95	16.80	3.83
25	15.66	17.04	15.29	15.99	5.75
26	158.87	159.27	155.28	157.80	1.39
27	195.51	193.59	184.39	191.16	3.11
28	185.38	185.52	185.69	185.53	0.09
29	197.39	197.63	194.32	196.45	0.94
30	158.11	156.35	160.38	158.28	1.28

Table B-2 TLDs measurement data for AP-PA fields: 10 MV.

Point	1 st Reading	2 nd Reading	3 rd Reading	Average	% RSD
1	18.33	18.48	18.04	18.28	1.22
2	173.15	173.98	174.19	173.77	0.32
3	177.51	180.78	182.00	180.09	1.29
4	182.78	188.25	190.15	187.06	2.04
5	187.26	194.33	195.75	192.45	2.36
6	166.27	167.31	167.79	167.12	0.46
7	8.51	8.51	8.41	8.48	0.69
8	19.50	19.23	18.50	19.08	2.71
9	149.72	152.69	153.23	151.88	1.25
10	149.84	147.69	148.17	148.57	0.76
11	167.68	167.69	166.06	167.14	0.56
12	174.62	175.64	177.26	175.84	0.76
13	184.79	187.13	186.54	186.15	0.65
14	177.42	179.46	180.30	179.06	0.83
15	177.27	181.18	181.01	179.82	1.23
16	191.62	193.79	196.37	193.93	1.23
17	187.00	189.00	189.72	188.57	0.75
18	187.23	190.76	190.94	189.64	1.10
19	193.77	193.93	196.28	194.66	0.72
20	197.92	196.71	196.59	197.07	0.37
21	183.14	183.76	184.23	183.71	0.30
22	187.98	187.45	188.92	188.12	0.40
23	141.41	147.64	160.12	149.72	6.36
24	18.20	18.61	19.13	18.65	2.50
25	16.34	15.27	15.61	15.74	3.47
26	158.66	153.56	153.40	155.21	1.93
27	170.04	163.54	165.10	166.23	2.04
28	171.64	174.27	170.98	172.30	1.01
29	186.93	181.37	180.53	182.94	1.90
30	154.57	151.85	157.44	154.62	1.81

Table B-3 TLDs measurement data for RAO-LPO fields: 6 MV.

Point	1 st Reading	2 nd Reading	3 rd Reading	Average	% RSD
1	234.51	235.91	232.13	234.18	0.82
2	186.18	189.10	187.92	187.73	0.78
3	181.92	178.00	181.45	180.46	1.19
4	183.65	184.92	182.08	183.55	0.78
5	212.43	216.63	213.95	214.34	0.99
6	234.24	235.39	237.36	235.66	0.67
7	18.65	18.70	18.41	18.59	0.84
8	205.91	204.80	203.62	204.78	0.56
9	186.71	191.16	186.04	187.97	1.48
10	143.76	144.60	143.12	143.83	0.52
11	217.99	221.90	221.78	220.56	1.01
12	205.51	208.21	205.84	206.52	0.71
13	191.41	194.69	190.74	192.28	1.10
14	185.23	187.54	187.47	186.75	0.70
15	162.66	160.87	164.00	162.51	0.97
16	174.27	179.66	179.91	177.95	1.79
17	192.38	190.65	193.17	192.06	0.67
18	205.55	207.10	207.60	206.75	0.52
19	16.33	17.59	16.12	16.68	4.74
20	245.38	249.13	241.36	245.29	1.58
21	195.96	200.68	195.38	197.34	1.47
22	181.07	186.17	179.98	182.41	1.81
23	189.79	195.01	187.46	190.75	2.03
24	214.75	222.42	207.87	215.02	3.39

Table B-4 TLDs measurement data for RAO-LPO fields: 10 MV.

Point	1 st Reading	2 nd Reading	3 rd Reading	Average	% RSD
1	209.15	208.89	207.69	208.57	0.37
2	185.24	186.55	188.76	186.85	0.95
3	174.92	180.71	184.41	180.01	2.66
4	183.78	187.02	191.19	187.33	1.98
5	206.13	208.14	209.01	207.76	0.71
6	212.32	214.66	214.05	213.68	0.57
7	16.75	16.41	16.36	16.51	1.30
8	198.53	196.40	198.36	197.76	0.60
9	184.42	183.57	183.74	183.91	0.25
10	134.58	124.97	133.01	130.85	3.94
11	208.04	208.33	213.70	210.02	1.52
12	201.95	203.52	204.15	203.21	0.56
13	189.54	190.04	192.00	190.53	0.68
14	187.85	186.41	186.24	186.83	0.47
15	155.45	150.30	155.33	153.69	1.91
16	164.57	172.61	172.83	170.00	2.77
17	185.11	188.03	193.98	189.04	2.39
18	201.35	208.45	208.24	206.01	1.96
19	17.05	17.81	17.73	17.53	2.38
20	202.95	205.84	204.34	204.37	0.71
21	191.89	188.10	187.70	189.23	1.22
22	181.57	179.29	177.84	179.57	1.05
23	190.17	188.29	182.86	187.11	2.03
24	204.33	199.31	199.44	201.03	1.42

BIOGRAPHY

NAME	Miss Wasuma Rakkrai
DATE OF BIRTH	7 August 1982
PLACE OF BIRTH	Pathumthani, Thailand
INSTITUTIONS ATTENDED	Mahidol University, 2004: Bachelor of science (Radiological Technology) Mahidol University, 2012: Master of science (Medical Physics)
HOME ADDRESS	42/7 Beungkumproi, lamlukka, Pathumthani 12150. Tel. 0865886788 E-mail: katevasuma@hotmail.com
EMPLOYMENT ADDRESS	Phramongkutkloa Hospital 315 Rajvithee Road, ratchathewi, Bangkok, Thailand 10400